Received: 8 February 2020 | Accepted: 24 January 2021

DOI: 10.1002/nme.6647

RESEARCH ARTICLE

WILEY

Acoustic scattering in nonhomogeneous media and the problem of discontinuous gradients: Analysis and inf-sup stability in the method of finite spheres

Williams L. Nicomedes[1] | **Klaus-Jürgen Bathe**[2] | **Fernando J. S. Moreira**[3] | **Renato C. Mesquita**[4]

[1]Graduate Program in Electrical Engineering, Federal University of Minas Gerais, Belo Horizonte, Brazil

[2]Department of Mechanical Engineering, Massachusetts Institute of Technology, Cambridge, Massachusetts, USA

[3]Department of Electronics Engineering, Federal University of Minas Gerais, Belo Horizonte, Brazil

[4]Department of Electrical Engineering, Federal University of Minas Gerais, Belo Horizonte, Brazil

Correspondence
Williams L. Nicomedes, Graduate Program in Electrical Engineering, Federal University of Minas Gerais, Belo Horizonte MG, 31270-901, Brazil.
Email: wnicomedes@eng-ele.grad.ufmg.br

Funding information
Conselho Nacional de Desenvolvimento Científico e Tecnológico (CNPq), Grant/Award Number: 150699/2019-0; Coordenação de Aperfeiçoamento de Pessoal de Nível Superior (CAPES)

Abstract

In this paper we focus on a meshfree formulation for the solution of time-harmonic acoustic scattering problems and verify the stability of the procedure. The sound waves propagate in nonhomogeneous media, giving rise to discontinuities in the gradients of the pressure field across the interfaces between regions of different material properties. Meshfree methods usually do not reproduce accurately the discontinuities in a numerical solution. We overcome this issue by introducing Lagrange multiplier fields defined at the interfaces in order to treat the discontinuities in the gradients of the pressure field. The method does not depend on any kind of adjustable parameter. We show by a numerical study of the applicable inf-sup conditions that the resulting mixed formulation leads to well-posed problems. The use of the proposed method is illustrated in the solution of a number of problems of wave propagation through nonhomogeneous media.

KEYWORDS

acoustic scattering, discontinuous gradients, finite elements, inf-sup conditions, meshfree methods, nonhomogeneous media

1 | INTRODUCTION

1.1 | Overview of the problem

Finite element methods (FEMs) constitute the most successful family of approximation methods in the numerical analysis and solution of models in computational mechanics.[1,2] Standard FEMs require meshing a geometric domain, usually into unstructured meshes.[1] Despite the fact that meshing techniques are experiencing an ever-increasing level of sophistication,[3] the creation of suitable finite element meshes can pose a challenge, particularly when complicated three-dimensional geometries are considered[4] or when frequent remeshing is necessary, as in crack propagation problems.[5-8] The possibility of avoiding meshing procedures motivated the introduction of a family of approximation methods, known collectively as *meshfree* or *meshless* methods.[9,10]

Among the different meshfree methods, the Smoothed Particle Hydrodynamics (SPH),[11] the Element-Free Galerkin (EFG),[12] the Meshless Local Petrov-Galerkin method (MLPG),[13] and the Method of Finite Spheres (MFS)[14] have since been applied to a range of problems. In this work, we use the MFS as the underlying meshfree method due to its demonstrated good performance in handling wave propagation problems.[15,16] A further development of the MFS is given by the overlapping finite elements (OFE), more recently proposed.[17-22] Since we use the MFS in this paper, the techniques discussed herein are also applicable to the OFE.

The propagation of linear sound waves (or electromagnetic waves in two dimensions) in the harmonic regime is described by the Helmholtz equation. Among the methods of solution, Boundary Element Methods (BEMs) are quite common.[23] These methods use a mesh over the surface/boundary of the computational domain only, so that the cost of producing a fully volumetric mesh (as in FEM) is eliminated. However, these methods are applicable only when the Green's function associated with the given differential operator is available. Even when it is available, difficulties with hypersingular integrals and non-uniqueness of solutions may occur, which demand special techniques of treatment.[24] BEMs are usually employed in the solution of fields in linear and homogeneous media, and lead to fully populated matrices. If we are interested in nonhomogeneous media (like those studied in this work), some transformations may be necessary.[25] Finite element methods of solution have also been proposed[26,27]; they can be extended to nonhomogeneous media, in addition to leading to sparse matrices.

In this work, we consider sound waves propagating in a homogeneous *host* medium, in which objects of different material properties are immersed. The properties (density and bulk modulus) are usually discontinuous across the interfaces separating the host medium and the objects. According to the corresponding physical model,[28,29] the discontinuity in the density leads to jumps in the gradient of the pressure field across the interfaces. The same phenomenon occurs in other scalar physical models (e.g., in the thermal analysis of polycrystals[30]).

1.2 | Finite elements and Lagrange multipliers

The standard FEM tackles this kind of problem by setting up a mesh which conforms to the interfaces, that is, a mesh in which the edges of the elements follow the contour of the interfaces. The construction of such a mesh may be challenging if the interfaces have complex boundaries, and the elements in the resulting mesh may have unacceptable aspect ratios.[30,31,32] It is possible to address this problem using the Generalized Finite Element Method (GFEM). The idea is to use enrichment functions that contain discontinuous gradients.[31,33] In this way, the edges of the elements do not need to conform to the interface. In fact, the interface just cuts through the elements, so that the resulting mesh can be constructed independently of the geometry of the interface.[30,32,34] A similar approach is used in embedded interface methods, where the discontinuity in the gradients is enforced using Nitsche's method.[35] The results are accurate, but stabilization parameters are required. The partition of unity finite element method (PUFEM) enriched with plane wave functions has also been considered.[36] Since the objects in the problem have different values for density (and bulk modulus), the plane waves have distinct wavenumbers within each object. Instead of defining approximation spaces with particular wavenumbers within each region and then applying some method to match the solution at the interfaces, all enrichment functions are combined into the same approximation space and applied over the entire computational domain. This approach yields good results, but if the problem is characterized by many objects with different material properties, the number of enrichment functions in the approximation space may become large.

Another tool popular with FEM is the use of Lagrange multipliers. They can be used to enforce boundary conditions and different types of interface conditions (such as jumps in constitutive laws across the interface,[37] and in contact problems[38]). The use of Lagrange multipliers leads to problems in mixed formulations, which must be solved for two fields simultaneously: The *primary field* (i.e., the field associated with the quantity we are interested in, such as pressure), and the *Lagrange multiplier field*. These fields cannot be approximated independently. The finite-dimensional subspaces used in the discretization of both fields must satisfy the corresponding *inf-sup conditions*. It is an established fact that a discrete problem is well-posed (its solution exists, is unique, and depends continuously on the data) if and only if the applicable inf-sup conditions (particular to each kind of problem) hold. Failure to satisfy the conditions leads to ill-posed discrete problems, and hence to numerical instabilities. More details can be found in authoritative discussions of this topic.[1,2,39,40,41]

Lagrange multipliers are used to impose Dirichlet boundary conditions in the extended finite element method (XFEM),[37] where a careful procedure is presented in order to construct a stable Lagrange multiplier space on the

boundary with the purpose of satisfying the inf-sup condition. These ideas are extended and compared to other techniques,[42] together with an algorithm (the vital vertex algorithm) proposed to construct a stable space for the Lagrange multipliers.

The use of Lagrange multipliers is also a popular procedure for the treatment of discontinuities in the solution and/or in its gradients. It is widely used in the context of finite element formulations,[43,44,45,46] discontinuous enrichment schemes (DE-FEMs),[47,48] XFEMs,[32] and discontinuous Galerkin methods (DG-FEMs).[49,50] In discontinuous Galerkin methods, the local approximation spaces defined within each element are discontinuous across element interfaces, and Lagrange multipliers are used to impose inter-element continuity of the solution. These methods usually require judicious selection of numerical fluxes and stabilization parameters.[51] Lagrange multipliers also play a prominent role in mortar methods,[52,53] and have also been used with the OFE method which, being based on the MFS, naturally can also carry enrichment functions.[22]

1.3 | Meshfree methods and discontinuous gradients

Despite the effectiveness of the FEMs described above, they all rely on meshes set over the domain prior to the discretization stage. Our aim in this paper is to conceive of a totally meshfree procedure able to solve problems whose solution may have discontinuous gradients.

There are many different meshfree methods, and distinct ways to classify them.[9,10,54] In this work, we shall focus on meshfree methods based on *weak forms*, or meshfree Galerkin methods, which are a suitable alternative to FEMs[55,56] (in opposition to meshfree methods based on *strong forms*, usually employed together with collocation procedures,[57] and which are a suitable alternative to finite difference methods).

If the solution of a problem is expected to exhibit discontinuous gradients across an interface, the application of meshfree Galerkin methods without any special procedure to treat the discontinuities leads to approximate solutions usually marked by some oscillations akin to Gibb's phenomenon close to the interface.[58] These oscillations usually begin at the curve's 'knee' and decrease as one moves away from the interface. There are at least three ways in which the discontinuous gradients can be treated in meshfree Galerkin methods. The first is based on the idea of *jump functions*.[58,59] Extra nodes are placed along the interface, with which certain jump functions are associated. These jump functions are included in the subspace used to approximate the solution. They are compactly supported and continuous across the interface. Their derivatives, on the other hand, must be discontinuous across the interface. The second way to treat discontinuous gradients is based on Lagrange multipliers.[60] The third way is the use of some penalty method,[61] which requires the specification of numerical parameters. Comparisons between jump functions and Lagrange multipliers,[60] and between Lagrange multipliers and penalty methods[61] have been made. The use of Lagrange multipliers yields slightly better results,[60] using also less quadrature points in the numerical integration. However, these works do not discuss the inf-sup conditions to be satisfied.

Our procedure is based on the MFS, which is a 'truly meshfree method'. Moreover, the basis (or shape) functions in the MFS are easier to construct than the basis functions in other meshfree methods, such as the moving least squares shape functions,[9] since inverting matrices is not necessary. The MFS has been applied thus far only to problems posed in media with homogeneous material properties.[14-16,62-71] In this work we choose an approach based on Lagrange multipliers and extend the MFS to problems for which discontinuous gradients are present in the solution. The resulting procedure is free of any stabilization parameter.

1.4 | Inf-sup testing

A rigorous derivation of the mixed problem associated with the Helmholtz equation, and specialized to the particular geometrical setting considered here, is presented in one of our works,[72] which is a companion paper to this one. In that work we show that the Lagrange multipliers arise naturally in the formulation, thus rendering this approach more straightforward to implement (since there are no 'amendments' like jump functions and tunable penalty factors). In the companion paper we also present a detailed derivation of the applicable inf-sup conditions. Once established, these conditions serve as the basis for the application of the inf-sup test, which is discussed in Sections 7 and 8 of the present work. This numerical test allows us to evaluate the well-posedness of the discrete problems as the discretization is refined.

1.5 | Organization of the manuscript

Section 2 discusses the physical model of the problem. The weak form of the governing equations is stated in Section 3. Section 4 is devoted to the meshfree discretization scheme, used in Section 5 for the numerical solutions of a number of boundary value problems. The well-posedness of the variational problem is discussed briefly in Section 6. The inf-sup stability analysis is formally discussed in Section 7. In Section 8, all problems from Section 5 are revisited, and their stability is assessed in the light of the results from the previous two sections. Concluding remarks are given in Section 9.

2 | THE PHYSICAL PROBLEM AND THE REFERENCE GEOMETRY USED

We state the problem considered and establish the model differential equations, for the interior of the domains and the boundary conditions. The corresponding variational equations are given in Section 3.

2.1 | Geometrical considerations

In order to make for a cleaner presentation, all aspects of the formulation and of the discretization process will be stated using the geometrical setting depicted in Figure 1 as a basis. The reasoning can be generalized to other geometrical settings, as long as their properties satisfy the assumptions made when constructing the model in Figure 1. When specialized to the setting in Figure 1, these assumptions become:

Assumption 1. In $\mathbb{R}^2$, we consider an open ball $B(\mathbf{0}; R)$, centered at the origin $\mathbf{0}$ and with a finite radius R. The boundary of this ball is denoted by Γ_R, see Figure 1.

Assumption 2. There is a collection of $M = 3$ regions, or objects, that is, bounded and open sets Ω_1, Ω_2, Ω_3, whose closures are contained within $B(\mathbf{0}; R)$ and do not touch Γ_R, see Figure 1.

Assumption 3. The regions Ω_1, Ω_2, Ω_3 are mutually disjoint.

Assumption 4. The region $\Omega_{M+1} = \Omega_4$ is defined as the set difference between $B(\mathbf{0}; R)$ and the union of the closures of all $M = 3$ regions, that is,

$$\Omega_4 \stackrel{\text{def}}{=} B(\mathbf{0}; R) \setminus \bigcup_{r=1}^{3} \overline{\Omega}_r, \tag{1}$$

The region Ω_4 represents the *host medium*.

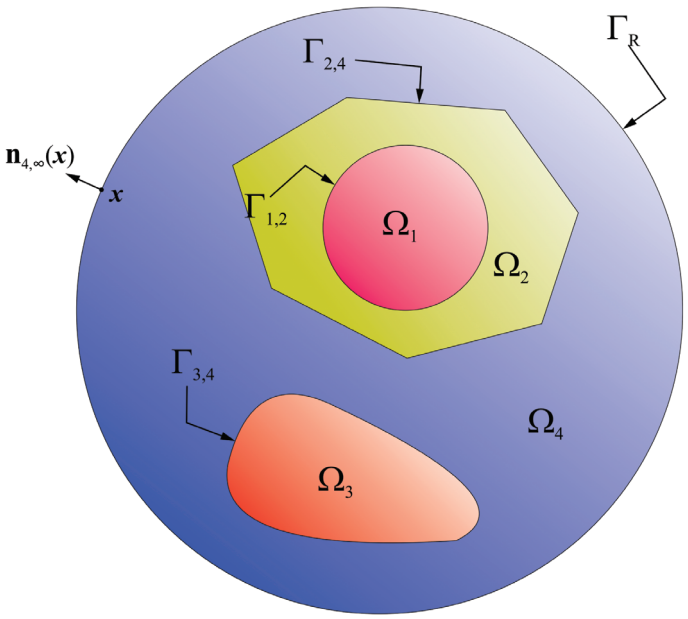

FIGURE 1 A setting with $M = 3$ objects, constructed according to the assumptions made in Section 2.1, resulting in a total of four regions (Ω_4 is the host medium). The interfaces $\Gamma_{1,2}$ (between regions Ω_1 and Ω_2), $\Gamma_{2,4}$ (between Ω_2 and Ω_4),and $\Gamma_{3,4}$ (between Ω_3 and Ω_4) are closed Lipschitz curves

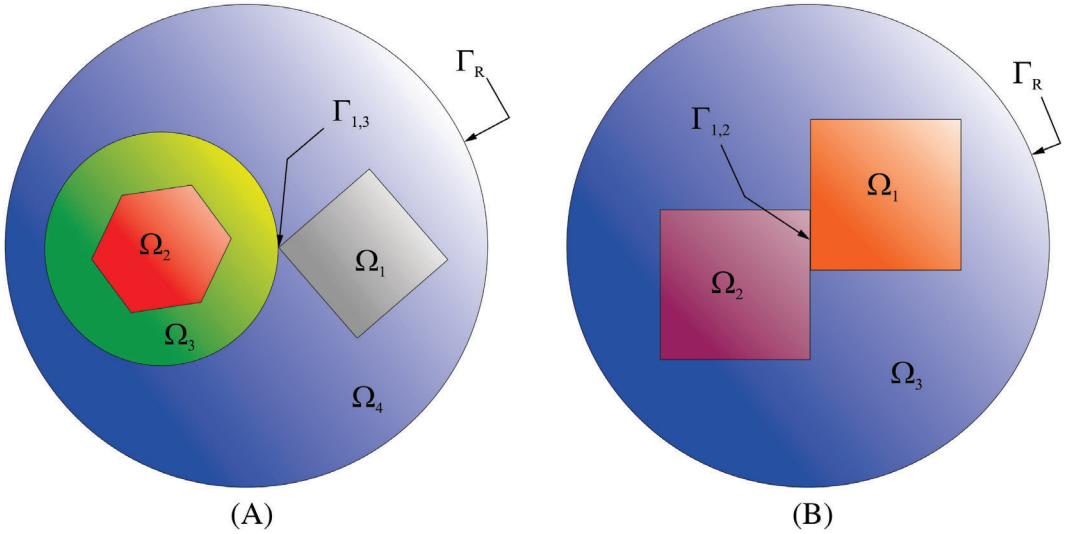

FIGURE 2 Examples of ruled out cases. (A) A setting for which $M = 3$. The intersection $\Gamma_{1,3}$ of $\partial\Omega_1$ and $\partial\Omega_3$ is a single point, and $\partial\Omega_4$ is not Lipschitz continuous. (B) A setting for which $M = 2$. The intersection $\Gamma_{1,2}$ of $\partial\Omega_1$ and $\partial\Omega_2$ is an open curve

Assumption 5. The boundary of each one of these $M+1 = 4$ regions is the union of a certain number of connected components ('pieces'). In the geometric setting from Figure 1, we have

$$\partial\Omega_1 = \Gamma_{1,2}, \tag{2a}$$

$$\partial\Omega_2 = \Gamma_{1,2} \cup \Gamma_{2,4}, \tag{2b}$$

$$\partial\Omega_3 = \Gamma_{3,4}, \tag{2c}$$

$$\partial\Omega_4 = \Gamma_{2,4} \cup \Gamma_{3,4} \cup \Gamma_R, \tag{2d}$$

where $\Gamma_{1,2}$ is the interface between regions Ω_1 and Ω_2. Interfaces $\Gamma_{2,4}$ and $\Gamma_{3,4}$ are defined in a similar manner. Each connected component in the problem must satisfy two properties: First, it is a *closed curve* (i.e., a curve whose endpoints coincide). Second, it can be decomposed into a finite number of arcs or line segments, that is, it has a finite number of vertices, see $\Gamma_{1,2}$ and $\Gamma_{2,4}$ in Figure 1. The component is then Lipschitz continuous.[73-75] Boundaries of not simply-connected regions (i.e., regions with holes, such as Ω_2 and Ω_4) have more than one connected component. The host medium is clearly not simply-connected.

Assumption 6. Considering the boundaries of all the $M+1 = 4$ regions, if we take any two of them, then only two mutually exclusive possibilities exist: First, they do not intersect (i.e., they are located at a certain distance from each other, such as $\partial\Omega_1$ and $\partial\Omega_3$ in Figure 1). Second, if they do intersect, then the intersection is a *single* closed curve (as $\partial\Omega_1$ and $\partial\Omega_2$ or $\partial\Omega_3$ and $\partial\Omega_4$ in Figure 1). We rule out the cases for which the intersection is a single point (as in Figure 2(A), which shows that $\partial\Omega_4$ fails to be Lipschitz continuous), or an open curve (i.e., a curve whose beginning and end points are different, as in Figure 2(B)).

2.2 | Equations of acoustic scattering

For each $r = 1, \cdots, 4$, we must solve the differential equation[29]: Find $p_r : \overline{\Omega}_r \longrightarrow \mathbb{C}$ such that for any $\boldsymbol{x} \in \Omega_r$,

$$\boldsymbol{\nabla} \cdot \left(\frac{1}{\rho_r(\boldsymbol{x})} \boldsymbol{\nabla} p_r(\boldsymbol{x}) \right) + \frac{\omega^2}{K_r(\boldsymbol{x})} p_r(\boldsymbol{x}) = 0, \tag{3}$$

where p_r is the phasor field associated with the time-harmonic pressure $\mathcal{p}_r(\boldsymbol{x}, t)$ (in $\mathrm{N/m^2}$). The latter can be recovered from the first via $\mathcal{p}_r(\boldsymbol{x}, t) = \mathrm{Re}\{p_r(\boldsymbol{x}) e^{j\omega t}\}$, where $\omega = 2\pi f$ is the angular frequency (in rad/s), f is the frequency (in Hz),

and Re{·} denotes the real part of a complex quantity. Moreover, $\rho_r : \Omega_r \longrightarrow \mathbb{R}^+$ is the density (in kg/m^3), and $K_r : \Omega_r \longrightarrow \mathbb{R}^+$ is the bulk modulus (in Pa) within region Ω_r.

In this work, we assume that the material filling up the host medium Ω_4 has constant density ρ_4 and bulk modulus K_4. We normalize the density and bulk modulus for all other regions, that is, we define, for all $r = 1, \cdots, 4$ and for $\boldsymbol{x} \in \Omega_r$,

$$\rho_{r,rel}(\boldsymbol{x}) \stackrel{\text{def}}{=} \rho_r(\boldsymbol{x})/\rho_4, \tag{4a}$$

$$K_{r,rel}(\boldsymbol{x}) \stackrel{\text{def}}{=} K_r(\boldsymbol{x})/K_4, \tag{4b}$$

where $\rho_{r,rel}$ and $K_{r,rel}$ are the 'relative' values of the density and bulk modulus with respect to the host medium Ω_4. Both $\rho_{r,rel}$ and $K_{r,rel}$ are dimensionless quantities. Substituting (4a) and (4b) in (3), we get a new set of equations: For each $r = 1, \cdots, 4$, find $p_r : \overline{\Omega}_r \longrightarrow \mathbb{C}$ such that for any $\boldsymbol{x} \in \Omega_r$,

$$\boldsymbol{\nabla} \cdot \left(\frac{1}{\rho_{r,rel}(\boldsymbol{x})} \boldsymbol{\nabla} p_r(\boldsymbol{x}) \right) + \frac{k^2}{K_{r,rel}(\boldsymbol{x})} p_r(\boldsymbol{x}) = 0, \tag{5}$$

where $k = \omega/c$ is the *wavenumber* associated with the host medium (in rad/m), and $c = \sqrt{K_4/\rho_4}$ is the speed of sound in the host medium.[29]

2.3 | Radiation boundary conditions

Because we assumed that both the density and the bulk modulus in the host medium are constant, it follows from (4a) and (4b) that $\rho_{4,rel}(\boldsymbol{x}) = K_{4,rel}(\boldsymbol{x}) = 1$, for any $\boldsymbol{x} \in \Omega_4$. Using this in (5) reveals that p_4 is governed by the homogeneous Helmholtz equation within Ω_4, that is, $\boldsymbol{\nabla}^2 p_4(\boldsymbol{x}) + k^2 p_4(\boldsymbol{x}) = 0$, for any $\boldsymbol{x} \in \Omega_4$.

The pressure p_4 can be decomposed into two parts: For any $\boldsymbol{x} \in \overline{\Omega}_4$, $p_4(\boldsymbol{x}) = p^{inc}(\boldsymbol{x}) + p^s(\boldsymbol{x})$, where $p^{inc} : \overline{\Omega}_4 \longrightarrow \mathbb{C}$ represents the *incident* pressure field. It is a function known in advance, and it must be chosen as one of the possible solutions of the Helmholtz equation within Ω_4, that is, $\boldsymbol{\nabla}^2 p^{inc}(\boldsymbol{x}) + k^2 p^{inc}(\boldsymbol{x}) = 0$, for any $\boldsymbol{x} \in \Omega_4$. In this work, possible sources for this field must be located outside the boundary Γ_R, see Figure 1. This incident field will be scattered, or perturbed by the materials immersed in the host medium. The result is the *scattered* pressure field $p^s : \overline{\Omega}_4 \longrightarrow \mathbb{C}$. It follows from the discussion above that p^s will also be a solution to the Helmholtz equation within Ω_4.

If Ω_4 were unbounded, that is, if the radius R became arbitrarily large (with $R \to \infty$), the correct boundary condition to be satisfied by p^s would be given by Sommerfeld's radiation condition,[26,28] which represents scattered waves propagating away from the origin. But since Ω_4 defined in (1) is bounded (R is finite, see Assumption 1 in Section 2.1), we use the approximate first-order Bayliss-Turkel absorbing boundary condition (ABC)[26,55,76] along the circle Γ_R. The condition to be satisfied by the total field p_4 thus becomes

$$\boldsymbol{\nabla} p_4(\boldsymbol{x}) \cdot \mathbf{n}_{4,\infty}(\boldsymbol{x}) + \left(jk + \frac{1}{2R} \right) p_4(\boldsymbol{x}) = F(\boldsymbol{x}), \tag{6a}$$

for all $\boldsymbol{x} \in \Gamma_R$. In (6a), $\mathbf{n}_{4,\infty}$ is the outward-pointing unit normal vector at $\boldsymbol{x}$ (see Figure 1), and the function F is given in terms of the incident field p^{inc}: For all $\boldsymbol{x} \in \Gamma_R$,

$$F(\boldsymbol{x}) \stackrel{\text{def}}{=} \boldsymbol{\nabla} p^{inc}(\boldsymbol{x}) \cdot \mathbf{n}_{4,\infty}(\boldsymbol{x}) + \left(jk + \frac{1}{2R} \right) p^{inc}(\boldsymbol{x}). \tag{6b}$$

2.4 | Interface conditions

The correct interface conditions[26,28,29] can be mathematically expressed as follows. If the assumptions made in the construction of the geometrical setting in Figure 1 are satisfied, then for the interface $\Gamma_{1,2}$, it is the case that the normal unit vector pointing from region Ω_1 into region Ω_2 is defined almost everywhere (a.e.)[74] along $\Gamma_{1,2}$, and is denoted by $\mathbf{n}_{1,2}$. Points in $\Gamma_{1,2}$ like vertices of polygons are excluded. For $\boldsymbol{x} \in \Gamma_{1,2}$ a.e., and for an arbitrarily small $\varepsilon > 0$, we define the two points:

$$\boldsymbol{x}_{1;\varepsilon} \stackrel{\text{def}}{=} \boldsymbol{x} - \varepsilon \mathbf{n}_{1,2}(\boldsymbol{x}), \quad \text{and} \quad \boldsymbol{x}_{2;\varepsilon} \stackrel{\text{def}}{=} \boldsymbol{x} + \varepsilon \mathbf{n}_{1,2}(\boldsymbol{x}), \tag{7a}$$

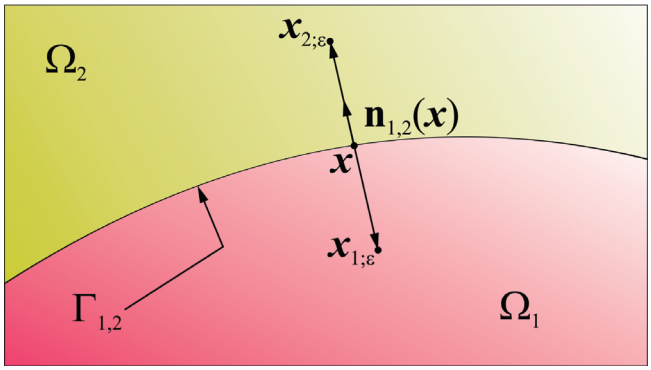

FIGURE 3 A closer look at the interface $\Gamma_{1,2}$ between regions Ω_1 and Ω_2. The normal unit vector pointing from region Ω_1 into region Ω_2 evaluated at $\boldsymbol{x} \in \Gamma_{1,2}$ is denoted by $\mathbf{n}_{1,2}(\boldsymbol{x})$. Given a small $\varepsilon > 0$, the points $\boldsymbol{x}_{1;\varepsilon} \in \Omega_1$ and $\boldsymbol{x}_{2;\varepsilon} \in \Omega_2$ in (7a) are shown

that is, point $\boldsymbol{x}_{1;\varepsilon}$ is in Ω_1, immediately 'below' $\Gamma_{1,2}$, and point $\boldsymbol{x}_{2;\varepsilon}$ is in Ω_2, immediately 'above' $\Gamma_{1,2}$ (see Figure 3). The first interface condition to be enforced along $\Gamma_{1,2}$ is:

$$\lim_{\varepsilon \to 0} \left(p_2(\boldsymbol{x}_{2;\varepsilon}) - p_1(\boldsymbol{x}_{1;\varepsilon}) \right) = 0, \tag{7b}$$

that is, the pressure field shall remain continuous as we move across the interface $\Gamma_{1,2}$. The second interface condition to be enforced along $\Gamma_{1,2}$ is:

$$\lim_{\varepsilon \to 0} \left(\frac{1}{\rho_{2,rel}(\boldsymbol{x}_{2;\varepsilon})} \nabla p_2(\boldsymbol{x}_{2;\varepsilon}) \cdot \mathbf{n}_{2,1}(\boldsymbol{x}) + \frac{1}{\rho_{1,rel}(\boldsymbol{x}_{1;\varepsilon})} \nabla p_1(\boldsymbol{x}_{1;\varepsilon}) \cdot \mathbf{n}_{1,2}(\boldsymbol{x}) \right) = 0, \tag{7c}$$

where $\mathbf{n}_{2,1}(\boldsymbol{x}) = -\mathbf{n}_{1,2}(\boldsymbol{x})$. Since the 'relative' densities $\rho_{1,rel}$ and $\rho_{2,rel}$ may assume different values at each side of the interface $\Gamma_{1,2}$, it is clear from (7c) that the gradients of the pressure fields p_1 and p_2 will be discontinuous. The two interface conditions to be enforced along $\Gamma_{2,4}$ and $\Gamma_{3,4}$ are obtained by the same reasoning, and are equal in form to (7b) and (7c).

3 | WEAK FORMS

The differential equations given above are in this section recast into variational form.

3.1 | Function spaces

The solution of the problem in strong form must be determined pointwise. We relax this requirement and look for weak solutions, which are expressed in terms of elements from Lebesgue and Sobolev spaces[77] specified over a given domain (an open and bounded subset) in $\mathbb{R}^2$. Elements from these spaces are not defined pointwise.[78,79] Moreover, throughout this paper, we are going to use only complex-valued versions of these spaces. Keeping the setting of Figure 1 in mind, given a region Ω_r, where $r = 1, \cdots, 4$, we write $L^2(\Omega_r)$ instead of $L^2(\Omega_r; \mathbb{C})$, and likewise for the other spaces.[80] Throughout this section, we remove the explicit dependence on position $\boldsymbol{x}$ in the equations. In Section 2.2, the pressure fields in the pointwise sense were defined up to the boundary of Ω_r (i.e., defined in the closure of Ω_r). In the weak case, the pressure fields are defined in the interior of Ω_r only; their behavior at the boundary $\partial\Omega_r$ is given by their traces. From now on we assume $p_r : \Omega_r \longrightarrow \mathbb{C}$. For all $r = 1, \cdots, 4$, we look for weak solutions p_r regular enough so that $p_r \in H^1(\Omega_r)$, and assume material properties regular enough to satisfy $(1/\rho_{r,rel}) \in C(\overline{\Omega}_r)$ and $(K_{r,rel}) \in C(\overline{\Omega}_r)$.[72] More details about the regularity of weak solutions to the Helmholtz equation can be found in the literature.[28,73,81] We next introduce the spaces $\mathcal{X}$ and $\mathcal{Y}$ defined as:

$$\mathcal{X} \stackrel{\text{def}}{=} H^1(\Omega_1) \times H^1(\Omega_2) \times H^1(\Omega_3) \times H^1(\Omega_4), \tag{8a}$$

$$\mathcal{Y} \stackrel{\text{def}}{=} H^{-1/2}(\Gamma_{1,2}) \times H^{-1/2}(\Gamma_{2,4}) \times H^{-1/2}(\Gamma_{3,4}). \tag{8b}$$

It is useful to represent vectors from the spaces $\mathcal{X}$ and $\mathcal{Y}$ by lowercase boldface letters, like:

$$\mathbf{v} \stackrel{\text{def}}{=} (v_1, v_2, v_3, v_4) \in \mathcal{X}, \tag{9a}$$

$$\boldsymbol{\mu} \overset{\text{def}}{=} (\mu_{1,2}, \mu_{2,4}, \mu_{3,4}) \in \mathcal{Y}. \tag{9b}$$

We equip these spaces with the following norms: For any $\mathbf{v} \in \mathcal{X}$, and for any $\boldsymbol{\mu} \in \mathcal{Y}$,

$$\|\mathbf{v}\|^2_{\mathcal{X}} \overset{\text{def}}{=} \|v_1\|^2_{H^1(\Omega_1)} + \|v_2\|^2_{H^1(\Omega_2)} + \|v_3\|^2_{H^1(\Omega_3)} + \|v_4\|^2_{H^1(\Omega_4)}, \tag{10a}$$

$$\|\boldsymbol{\mu}\|^2_{\mathcal{Y}} \overset{\text{def}}{=} \|\mu_{1,2}\|^2_{H^{-1/2}(\Gamma_{1,2})} + \|\mu_{2,4}\|^2_{H^{-1/2}(\Gamma_{2,4})} + \|\mu_{3,4}\|^2_{H^{-1/2}(\Gamma_{3,4})}. \tag{10b}$$

The standard norm[41,78,80] in the H^1 space is given by:

$$\|v_1\|^2_{H^1(\Omega_1)} \overset{\text{def}}{=} \int_{\Omega_1} (\boldsymbol{\nabla} v_1 \cdot \boldsymbol{\nabla} v_1^* + v_1 v_1^*) d\Omega, \tag{11a}$$

and likewise for the other terms in (10a). The standard norm in the $H^{-1/2}$ space is given by

$$\|\mu_{1,2}\|_{H^{-1/2}(\Gamma_{1,2})} \overset{\text{def}}{=} \sup_{\substack{t \in H^{1/2}(\Gamma_{1,2}) \\ t \neq 0}} \frac{|\langle\, \mu_{1,2} \mid t \,\rangle_{H^{1/2}(\Gamma_{1,2})}|}{\|t\|_{H^{1/2}(\Gamma_{1,2})}}. \tag{11b}$$

The norm $\|\cdot\|_{H^{-1/2}(\Gamma_{1,2})}$ defined in (11b) is a *dual norm* (since $H^{-1/2}$ is the dual space of $H^{1/2}$). The term $\langle\, \mu_{1,2} \mid t \,\rangle_{H^{1/2}(\Gamma_{1,2})}$ represents the duality pairing[80] between the functional $\mu_{1,2} \in H^{-1/2}(\Gamma_{r,s})$ and the function $t \in H^{1/2}(\Gamma_{1,2})$. The norm $\|\cdot\|_{H^{1/2}(\Gamma_{1,2})}$ in (11b) is given in Appendix B. The $H^{-1/2}$ norm of the other terms in (10b) are calculated likewise.

3.2 | The problem in weak form

The problem in weak form consists in finding a vector of pressure fields $\mathbf{p} \overset{\text{def}}{=} (p_1 p_2 p_3 p_4) \in \mathcal{X}$, and a vector of Lagrange multiplier fields $\boldsymbol{\lambda} \overset{\text{def}}{=} (\lambda_{1,2} \lambda_{2,4} \lambda_{3,4}) \in \mathcal{Y}$. After a lengthy reasoning,[72] and considering geometrical domains in which the assumptions made in Section 2.1 hold true, it can be shown that the weak problem derived from (5), (6a), and the interface conditions discussed in Section 2.4 is given by

$$\begin{aligned} &\text{Find } (\mathbf{p}, \boldsymbol{\lambda}) \in \mathcal{X} \times \mathcal{Y} \text{ such that} \\ &a(\mathbf{p}, \mathbf{v}) + b(\mathbf{v}, \boldsymbol{\lambda}) = \langle Q' \mid \mathbf{v} \rangle_{\mathcal{X}^\star, \mathcal{X}}, \text{for any } \mathbf{v} \in \mathcal{X}, \\ &b(\mathbf{p}, \boldsymbol{\mu}) = 0, \text{for any } \boldsymbol{\mu} \in \mathcal{Y}. \end{aligned} \tag{12a}$$

In (12a), the bilinear form $a : \mathcal{X} \times \mathcal{X} \longrightarrow \mathbb{C}$ is given by:

$$a(\mathbf{w}, \mathbf{v}) \overset{\text{def}}{=} \sum_{r=1}^{4} \int_{\Omega_r} \left(\frac{1}{\rho_{r,rel}} \boldsymbol{\nabla} v_r \cdot \boldsymbol{\nabla} w_r - \frac{k^2}{K_{r,rel}} v_r w_r \right) d\Omega + \int_{\Gamma_R} \left(jk + \frac{1}{2R} \right) (\gamma_{\partial\Omega_4}(v_4))|_{\Gamma_R} (\gamma_{\partial\Omega_4}(w_4))|_{\Gamma_R} d\Gamma, \tag{12b}$$

for any $(\mathbf{w}, \mathbf{v}) \in \mathcal{X} \times \mathcal{X}$. The term $\gamma_{\partial\Omega_4}(w_4)$ represents the (interior) trace of w_4 along $\partial\Omega_4$. Since $w_4 \in H^1(\Omega_4)$, it follows from the Trace theorem (Appendix A) that this trace belongs to $H^{1/2}(\partial\Omega_4)$. Its restriction to $\Gamma_R \subset \partial\Omega_4$ belongs to $H^{1/2}(\Gamma_R)$, see Appendix B. The same applies to the term $\gamma_{\partial\Omega_4}(v_4)$. The bilinear form $b : \mathcal{X} \times \mathcal{Y} \longrightarrow \mathbb{C}$ is given by

$$\begin{aligned} b(\mathbf{v}, \boldsymbol{\mu}) \overset{\text{def}}{=} &\langle\, \mu_{1,2} \mid \gamma_{\partial\Omega_2}(v_2)|_{\Gamma_{1,2}} - \gamma_{\partial\Omega_1}(v_1) \,\rangle_{H^{1/2}(\Gamma_{1,2})} \\ &+ \langle\, \mu_{2,4} \mid \gamma_{\partial\Omega_4}(v_4)|_{\Gamma_{2,4}} - \gamma_{\partial\Omega_2}(v_2)|_{\Gamma_{2,4}} \,\rangle_{H^{1/2}(\Gamma_{2,4})} \\ &+ \langle\, \mu_{3,4} \mid \gamma_{\partial\Omega_4}(v_4)|_{\Gamma_{3,4}} - \gamma_{\partial\Omega_3}(v_3) \,\rangle_{H^{1/2}(\Gamma_{3,4})}, \end{aligned} \tag{12c}$$

for any $(\mathbf{v}\boldsymbol{\mu}) \in \mathcal{X} \times \mathcal{Y}$. The term $\gamma_{\partial\Omega_2}(v_2)$ represents the trace of v_2 along $\partial\Omega_2$. Since $v_2 \in H^1(\Omega_2)$, it follows from the Trace theorem that this trace belongs to $H^{1/2}(\partial\Omega_2)$. Moreover, since $\Gamma_{1,2} \subset \partial\Omega_2$ according to (2b), it follows that the restriction of the trace $\gamma_{\partial\Omega_2}(v_2)$ to $\Gamma_{1,2}$ belongs to $H^{1/2}(\Gamma_{1,2})$. The other traces in (12c) are treated similarly. Finally, the functional Q'

is defined as: For any $\mathbf{v} \in \mathcal{X}$,

$$Q'(\mathbf{v}) \stackrel{\text{def}}{=} \int_{\Gamma_R} (\gamma_{\partial\Omega_4}(v_4))|_{\Gamma_R} F \, d\Gamma, \tag{12d}$$

where the function F is given in (6b). It can be shown that if $F \in L^2(\Gamma_R)$, then the functional Q' is linear and bounded, that is, there is a constant $C_1 > 0$ such that $|Q'(\mathbf{v})| \leq C_1 \|\mathbf{v}\|_{\mathcal{X}}$, for any $\mathbf{v} \in \mathcal{X}$. In this way, Q' belongs to $\mathcal{X}^\star$, the dual space of $\mathcal{X}$. Using duality pairing, we therefore write $\langle\, Q' \mid \mathbf{v} \,\rangle_{\mathcal{X}^\star,\mathcal{X}} = Q'(\mathbf{v})$, for any $\mathbf{v} \in \mathcal{X}$. It can also be shown from (6b) that if the incident field p^{inc} is given by plane wave solutions of the type $p^{inc}(\boldsymbol{x}) = e^{-j\boldsymbol{k}\cdot\boldsymbol{x}}$, where $\boldsymbol{k} = k\widehat{\boldsymbol{k}}$ and $\boldsymbol{x} = [x, y]$, then $F \in L^2(\Gamma_R)$. In this last expression, $\widehat{\boldsymbol{k}}$ is a unit vector in the direction the plane wave propagates. The problem (12a) is cast in what is called a *mixed formulation*.[1,39,40,41,82]

4 | MESHFREE DISCRETIZATION PROCESS

There are many meshfree discretization schemes, some still require a background mesh for the numerical integration, like the EFG method.[12] We use the MFS which is a truly meshfree procedure.

4.1 | Method of finite spheres

The discretization process adopted in this work follows the guidelines outlined in the MFS.[14-16,62,69-71] The MFS is a Galerkin method with local enrichment properties. It is a totally meshfree method (in the sense that the numerical integrations are carried out locally in the subdomains). In the aforementioned references, the MFS showed a good performance when applied to problems posed in homogeneous media. We now extend it to nonhomogeneous media.

4.2 | Meshfree finite dimensional subspaces for the pressure fields

For each $r = 1, \cdots, 4$, a *finite sphere system* over region Ω_r is the pair

$$\mathcal{FS}(\Omega_r) \stackrel{\text{def}}{=} (\mathcal{B}(\Omega_r), \mathcal{M}(\Omega_r)), \tag{13a}$$

where $\mathcal{B}(\Omega_r) = \{B(r_1; \boldsymbol{x}_1), B(r_2; \boldsymbol{x}_2) \cdots\}$ is a *finite* collection of (overlapping) open balls, each one centered at point $\boldsymbol{x}_i = (x_i, y_i)$ and with radius r_i, see Figure 4. The number of balls (also called *subdomains*, or *spheres*) in $\mathcal{B}(\Omega_r)$ is denoted by $|\mathcal{B}(\Omega_r)|$. The union of all balls in $\mathcal{B}(\Omega_r)$ is represented by U_r, and must cover the closure[14] of Ω_r, that is,

$$\overline{\Omega}_r \subset U_r \stackrel{\text{def}}{=} \bigcup_{i=1}^{|\mathcal{B}(\Omega_r)|} B(r_i; \boldsymbol{x}_i). \tag{13b}$$

The element $\mathcal{M}(\Omega_r)$ in (13a) is a meshfree finite-dimensional subspace of real-valued functions spanned by the basis functions defined on Ω_r.

In order to construct $\mathcal{M}(\Omega_r)$, we first choose a relatively smooth real-valued weight function $w : [0, \infty) \longrightarrow [0, \infty)$, such as the quartic spline[9]: For any $t \in [0, \infty)$,

$$w(t) = \begin{cases} 1 - 6t^2 + 8t^3 - 3t^4, & t \in [0, 1], \\ 0, & t \in (1, \infty). \end{cases} \tag{14a}$$

The support of the weight function (14a) is supp $w = [0, 1]$. Both w and its first derivative are continuous on $[0, \infty)$, and therefore $w \in C^1([0, \infty))$. First we associate with each ball $B(r_i; \boldsymbol{x}_i)$ the *transformed weight function* $\widetilde{w}_i^r$, defined as

$$\widetilde{w}_i^r(\boldsymbol{x}) \stackrel{\text{def}}{=} w\left(\frac{\|\boldsymbol{x} - \boldsymbol{x}_i\|}{r_i}\right), \tag{14b}$$

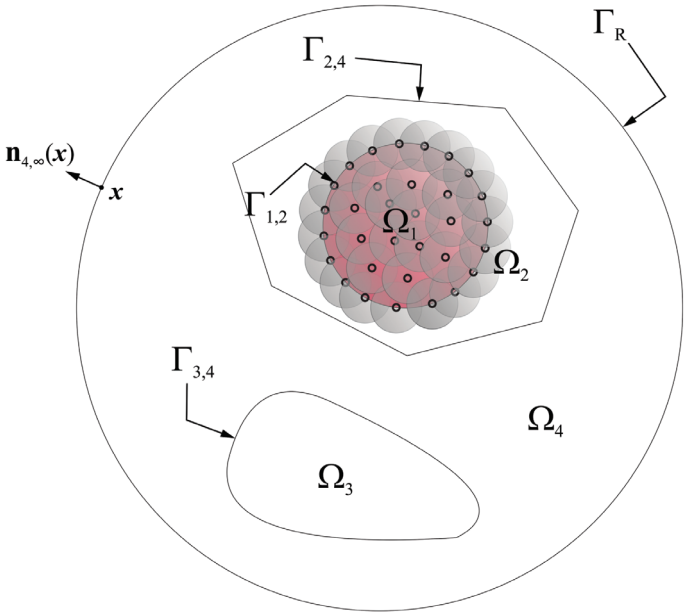

FIGURE 4 The same setting from Figure 1. We see the collection of balls $\mathcal{B}(\Omega_1)$, whose union U_1 covers $\overline{\Omega}_1$ (closure of region Ω_1). In the same way, separate collections of balls must be set up in order to cover $\overline{\Omega}_2$, $\overline{\Omega}_3$, and $\overline{\Omega}_4$ (not shown)

for any $\boldsymbol{x} \in \mathbb{R}^2$, where $\| \bullet \|$ denotes the Euclidean norm of a vector in $\mathbb{R}^2$. Since supp $w = [0, 1]$, it follows that supp $\widetilde{w}_i^r = \{\boldsymbol{x} \in \mathbb{R}^2 | \, \|\boldsymbol{x} - \boldsymbol{x}_i\| \leq r_i\}$, that is, the closure of the ith ball. It can be shown that each $\widetilde{w}_i^r \in C^1(\mathbb{R}^2)$. After all transformed weight functions have been constructed, a collection of *partition of unity* (PU) functions can be defined. Next we associate with each ball $B(r_i; \boldsymbol{x}_i)$ the PU function φ_i^r,defined as

$$\varphi_i^r(\boldsymbol{x}) \stackrel{\text{def}}{=} \widetilde{w}_i^r(\boldsymbol{x}) / \sum_{j=1}^{|\mathcal{B}(\Omega_r)|} \widetilde{w}_j^r(\boldsymbol{x}), \tag{14c}$$

for any $\boldsymbol{x} \in U_r$. The domain of definition of φ_i^r is the union U_r. (Outside of U_r, the denominator in (14c) is zero). It can be verified that both φ_i^r and its derivatives are continuous on all of U_r, that is, $\varphi_i^r \in C^1(U_r)$. The support of the PU function φ_i^r is also given by the closure of ball $B(r_i; \boldsymbol{x}_i)$. With each ball $B(r_i; \boldsymbol{x}_i)$ in $\mathcal{B}(\Omega_r)$, we also associate a collection $\mathscr{L}(U_r; i)$ of six linearly independent *local enrichment functions*, that is, $\mathscr{L}(U_r; i) = \{l_{i,1}^r l_{i,2}^r l_{i,3}^r l_{i,4}^r l_{i,5}^r l_{i,6}^r\}$, where $l_{i,m}^r : U_r \longrightarrow \mathbb{R}$, $m = 1, \cdots, 6$. The elements from $\mathscr{L}(U_r; i)$ are defined as: For any $\boldsymbol{x} \in U_r$,

$$\begin{aligned} l_{i,1}^r(\boldsymbol{x}) &\stackrel{\text{def}}{=} 1, & l_{i,2}^r(\boldsymbol{x}) &\stackrel{\text{def}}{=} (x - x_i)/r_i, & l_{i,4}^r(\boldsymbol{x}) &\stackrel{\text{def}}{=} (x - x_i)^2/r_i^2, \\ & & l_{i,3}^r(\boldsymbol{x}) &\stackrel{\text{def}}{=} (y - y_i)/r_i, & l_{i,5}^r(\boldsymbol{x}) &\stackrel{\text{def}}{=} (x - x_i)(y - y_i)/r_i^2, \\ & & & & l_{i,6}^r(\boldsymbol{x}) &\stackrel{\text{def}}{=} (y - y_i)^2/r_i^2. \end{aligned} \tag{15}$$

For each function $l_{i,m}^r$ listed above, it can be verified that both $l_{i,m}^r$ and its derivatives are continuous on all of U_r, that is, $l_{i,m}^r \in C^1(U_r)$. The meshfree finite-dimensional subspace $\mathcal{M}(\Omega_r)$ introduced in (13a) is defined as

$$\mathcal{M}(\Omega_r) \stackrel{\text{def}}{=} \text{span}\, \{h_{i,m}^r : i = 1, \cdots, |\mathcal{B}(\Omega_r)|, \quad \text{and} \quad m = 1, \cdots, 6\}, \tag{16}$$

where each basis function $h_{i,m}^r : \Omega_r \longrightarrow \mathbb{R}$ (indexed by i and m) is given by the restriction of the product $\varphi_i^r l_{i,m}^r$ to Ω_r, that is, $h_{i,m}^r \stackrel{\text{def}}{=} (\varphi_i^r l_{i,m}^r)|_{\Omega_r}$, or equivalently, $h_{i,m}^r(\boldsymbol{x}) = \varphi_i^r(\boldsymbol{x}) l_{i,m}^r(\boldsymbol{x})$, for any point $\boldsymbol{x} \in \Omega_r$. The collection of basis functions $h_{i,m}^r$ just defined is linearly independent,[14] and the dimension of space $\mathcal{M}(\Omega_r)$ is dim $\mathcal{M}(\Omega_r) = 6|\mathcal{B}(\Omega_r)|$. The support of the basis function $h_{i,m}^r$ is the closure of the intersection between the ball $B(r_i; \boldsymbol{x}_i)$ and the region Ω_r. Since this ball is usually much smaller than the domain Ω_r (see Figure 4), the basis function $h_{i,m}^r$ is zero over a large portion of Ω_r. The typical form of these basis functions can be seen in some of the references.[14,62] The basis function $h_{i,m}^r$ belongs to $H^1(\Omega_r)$.[14] This implies that its trace $\gamma_{\partial\Omega_r}(h_{i,m}^r)$ along the boundary $\partial\Omega_r$ belongs to $H^{1/2}(\partial\Omega_r)$. Due to the smoothness of the product $\varphi_i^r l_{i,m}^r$, it can be

shown that the resulting basis function $h^r_{i,m}$ also belongs to the space $C^{0,1}(\overline{\Omega}_r)$, and therefore its trace is well defined and given by the continuous extension of $h^r_{i,m}$ to the boundary $\partial\Omega_r$ (see Appendix A). An arbitrary function $v_{r;h}$ from $\mathcal{M}(\Omega_r)$ can therefore be represented as

$$v_{r;h} = \mathbf{H}_r^T \widetilde{\mathbf{V}}_r, \tag{17a}$$

where the vector function $\mathbf{H}_r : \Omega_r \longrightarrow \mathbb{R}^{\dim \mathcal{M}(\Omega_r)}$ collects all basis functions $h^r_{i,m}$ (i.e., the function $\mathbf{H}_r$ receives a point $\boldsymbol{x} \in \Omega_r$ and returns a vector in $\mathbb{R}^{\dim \mathcal{M}(\Omega_r)}$ whose ith component is given by $h^r_{i,m}(\boldsymbol{x}) = \varphi^r_i(\boldsymbol{x}) l^r_{i,m}(\boldsymbol{x})$), and $\widetilde{\mathbf{V}}_r \in \mathbb{C}^{\dim \mathcal{M}(\Omega_r)}$ is a (column) vector of coefficients. The trace of $v_{r;h}$ along the boundary $\partial\Omega_r$ is represented as

$$\gamma_{\partial\Omega_r}(v_{r;h}) = \mathbf{T}_r^T \widetilde{\mathbf{V}}_r, \tag{17b}$$

where the vector function $\mathbf{T}_r : \partial\Omega_r \longrightarrow \mathbb{R}^{\dim \mathcal{M}(\Omega_r)}$ collects the traces of all basis functions $h^r_{i,m}$ along the boundary $\partial\Omega_r$ (i.e., $\mathbf{T}_r$ receives a point $\boldsymbol{x} \in \partial\Omega_r$ and returns a vector in $\mathbb{R}^{\dim \mathcal{M}(\Omega_r)}$ whose ith component is given by $(\gamma_{\partial\Omega_r}(h^r_{i,m}))(\boldsymbol{x}) = \varphi^r_i(\boldsymbol{x}) l^r_{i,m}(\boldsymbol{x})$, since $h^r_{i,m}$ can be continuously extended to the boundary). In addition to the trace along $\partial\Omega_r$, the gradient of $v_{r;h}$ is calculated via the matrix function $\overline{\mathbf{G}}_r : \Omega_r \longrightarrow \mathbb{R}^{\dim \mathcal{M}(\Omega_r)\times 2}$ as

$$\boldsymbol{\nabla} v_{r;h} = \widetilde{\mathbf{V}}_r^T \overline{\mathbf{G}}_r = \widetilde{\mathbf{V}}_r^T \left[\frac{\partial \mathbf{H}_r}{\partial x}, \ \frac{\partial \mathbf{H}_r}{\partial y} \right]. \tag{17c}$$

After all finite sphere systems $\mathcal{FS}(\Omega_1), \cdots, \mathcal{FS}(\Omega_4)$ in (13a) have been constructed, we define a finite dimensional subspace $\mathcal{X}_h$ of $\mathcal{X}$ in (8a) as:

$$\mathcal{X}_h \stackrel{\text{def}}{=} \mathcal{M}(\Omega_1) \times \mathcal{M}(\Omega_2) \times \mathcal{M}(\Omega_3) \times \mathcal{M}(\Omega_4). \tag{18a}$$

The norm in $\mathcal{X}_h$ is that inherited from $\mathcal{X}$ in (10a). Since $\dim \mathcal{M}(\Omega_r) = 6|\mathcal{B}(\Omega_r)|$ (see above), the dimension of $\mathcal{X}_h$ is

$$\dim \mathcal{X}_h = \sum_{r=1}^{4} \dim \mathcal{M}(\Omega_r) = 6 \sum_{r=1}^{4} |\mathcal{B}(\Omega_r)|. \tag{18b}$$

4.3 | Meshfree finite dimensional subspaces for the Lagrange multiplier fields

Since the Lagrange multiplier fields in problem (12a) are functionals (and not functions), we present a way to construct meshfree spaces of functionals. The Lagrange multiplier fields are elements of the space $\mathcal{Y}$ in (8b), and we consider now how the discretized versions of the functionals in the individual spaces $H^{-1/2}(\Gamma_{1,2})$, $H^{-1/2}(\Gamma_{2,4})$, and $H^{-1/2}(\Gamma_{3,4})$ can be characterized. We shall focus on the space $H^{-1/2}(\Gamma_{1,2})$ first. A finite sphere system over the interface $\Gamma_{1,2}$ is the pair

$$\mathcal{FS}(\Gamma_{1,2}) \stackrel{\text{def}}{=} (\mathcal{B}(\Gamma_{1,2}), \mathcal{M}(\Gamma_{1,2})), \tag{19}$$

which is constructed exactly as described in Section 4.2. The union $U_{1,2}$ of all balls in the collection $\mathcal{B}(\Gamma_{1,2})$ must cover the curve $\Gamma_{1,2}$, that is, $\Gamma_{1,2} \subset U_{1,2}$, see Figure 5. With each ball $B(r_i; \boldsymbol{x}_i)$ in $\mathcal{B}(\Gamma_{1,2})$ we associate a transformed weight function as in (14b); after these weight functions are defined, we construct a collection of PU functions $\varphi^{1,2}_i : U_{1,2} \longrightarrow \mathbb{R}$, $i = 1, \cdots |\mathcal{B}(\Gamma_{1,2})|$ (one for each ball) as in (14c). However, with each ball $B(r_i; \boldsymbol{x}_i)$ in $\mathcal{B}(\Gamma_{1,2})$, we associate only one constant *local enrichment function*, that is, we make $\mathscr{L}(U_{1,2}; i) = \{l^{1,2}_{i,1}\}$, where $l^{1,2}_{i,1}(\boldsymbol{x}) \stackrel{\text{def}}{=} 1$, for any $\boldsymbol{x} \in U_{1,2}$. The meshfree finite-dimensional subspace $\mathcal{M}(\Gamma_{1,2})$ introduced in (19) is defined as

$$\mathcal{M}(\Gamma_{1,2}) \stackrel{\text{def}}{=} \text{span}\{h^{1,2}_i : i = 1, \cdots, |\mathcal{B}(\Gamma_{1,2})|\}, \tag{20}$$

where the basis function $h^{1,2}_i : \Gamma_{1,2} \longrightarrow \mathbb{R}$ (indexed by i only) is given by the restriction of the product $\varphi^{1,2}_i l^{1,2}_{i,1} = \varphi^{1,2}_i$ to $\Gamma_{1,2}$, that is, $h^{1,2}_i \stackrel{\text{def}}{=} \varphi^{1,2}_i|_{\Gamma_{1,2}}$, or equivalently, $h^{1,2}_i(\boldsymbol{x}) \stackrel{\text{def}}{=} \varphi^{1,2}_i(\boldsymbol{x})$, for any point $\boldsymbol{x} \in \Gamma_{1,2}$. The dimension of space $\mathcal{M}(\Gamma_{1,2})$ is therefore $\dim \mathcal{M}(\Gamma_{1,2}) = |\mathcal{B}(\Gamma_{1,2})|$, that is, equal to the number of balls in $\mathcal{B}(\Gamma_{1,2})$. The support of the basis function $h^{1,2}_i$ is the closure of the intersection between the ball $B(r_i; \boldsymbol{x}_i)$ and the curve $\Gamma_{1,2}$. This ball is usually much smaller than $\Gamma_{1,2}$ (see Figure 5), and consequently $h^{1,2}_i$ is zero over a large portion of $\Gamma_{1,2}$. Using the notion of tangential gradients[83,84] along the curve $\Gamma_{1,2}$, it can be shown that the basis function $h^{1,2}_i$ belongs to $H^1(\Gamma_{1,2})$. We use the fact[41] that $H^1(\Gamma_{1,2}) \subset H^{1/2}(\Gamma_{1,2})$

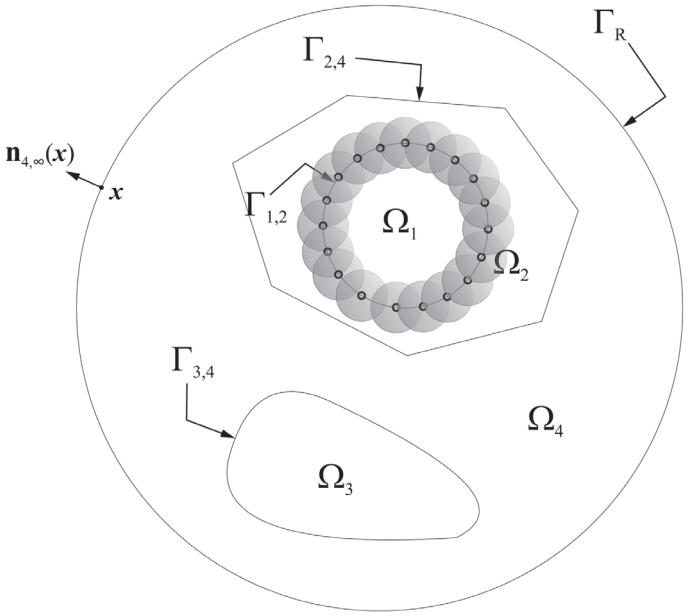

FIGURE 5 The interface between regions Ω_1 and Ω_2 is given by the closed curve $\Gamma_{1,2}$. We show the collection of balls $\mathcal{B}(\Gamma_{1,2})$, whose union $U_{1,2}$ covers $\Gamma_{1,2}$. Separate collections of balls must also be set up in order to cover the interfaces $\Gamma_{2,4}$ and $\Gamma_{3,4}$ (not shown)

to conclude that $h_i^{1,2} \in H^{1/2}(\Gamma_{1,2})$, for $i = 1, \cdots |\mathcal{B}(\Gamma_{1,2})|$. With each basis function $h_i^{1,2}$, we can associate the functional $\tau_i^{1,2} \in H^{-1/2}(\Gamma_{1,2})$ characterized as:

$$\langle\, \tau_i^{1,2} \mid v \,\rangle_{H^{1/2}(\Gamma_{1,2})} \stackrel{\text{def}}{=} \int_{\Gamma_{1,2}} h_i^{1,2} v \, d\Gamma, \tag{21}$$

for any $v \in H^{1/2}(\Gamma_{1,2})$. We define a meshfree space of functionals as

$$\mathcal{M}(\Gamma_{1,2})' \stackrel{\text{def}}{=} \text{span}\{\tau_i^{1,2} \,:\, i = 1, \cdots, |\mathcal{B}(\Gamma_{1,2})|\}. \tag{22}$$

The collection of basis functions $h_i^{1,2}$ is linearly independent, and it can be shown that the collection of functionals $\tau_i^{1,2}$ is also linearly independent. Therefore, $\dim \mathcal{M}(\Gamma_{1,2})' = \dim \mathcal{M}(\Gamma_{1,2}) = |\mathcal{B}(\Gamma_{1,2})|$. Since each $\tau_i^{1,2}$ belongs to $H^{-1/2}(\Gamma_{1,2})$, it follows that $\mathcal{M}(\Gamma_{1,2})'$ is a finite-dimensional subspace of $H^{-1/2}(\Gamma_{1,2})$. Let $\mu_{1,2;h}$ be a generic functional from the space $\mathcal{M}(\Gamma_{1,2})'$ in (22), which can be expressed as a linear combination of functionals $\tau_i^{1,2}$ as

$$\mu_{1,2;h} = \sum_{i=1}^{|\mathcal{B}(\Gamma_{1,2})|} \tau_i^{1,2} \, \widetilde{u}_i^{1,2}, \tag{23a}$$

where $\widetilde{u}_i^{1,2} \in \mathbb{C}$ denotes the ith expansion coefficient. Using (21) and (23a), it is straightforward to show that the action of $\mu_{1,2;h}$ on an arbitrary function $v \in H^{1/2}(\Gamma_{1,2})$ is given by

$$\langle\, \mu_{1,2;h} \mid v \,\rangle_{H^{1/2}(\Gamma_{1,2})} = \widetilde{\mathbf{U}}_{1,2}^T \int_{\Gamma_{1,2}} \mathbf{H}_{1,2} v \, d\Gamma. \tag{23b}$$

In (23b), all basis functions $h_i^{1,2}$ have been ordered and collected into a vector function $\mathbf{H}_{1,2} : \Gamma_{1,2} \longrightarrow \mathbb{R}^{\dim \mathcal{M}(\Gamma_{1,2})}$, that is, the function $\mathbf{H}_{1,2}$ receives a point $\boldsymbol{x} \in \Gamma_{1,2}$ and returns a vector of real numbers whose ith component is given by $h_i^{1,2}(\boldsymbol{x}) = \varphi_i^{1,2}(\boldsymbol{x})$. The expansion coefficients have also been ordered and collected into the vector $\widetilde{\mathbf{U}}_{1,2} \in \mathbb{C}^{\dim \mathcal{M}(\Gamma_{1,2})}$.

The same procedure described above can be applied to the interfaces $\Gamma_{2,4}$ and $\Gamma_{3,4}$ in order to construct the finite-sphere systems $\mathcal{FS}(\Gamma_{2,4})$ and $\mathcal{FS}(\Gamma_{3,4})$, respectively. In complete analogy with (23b), if the generic functionals $\mu_{2,4;h}$ and $\mu_{3,4;h}$ from the meshfree subspaces $\mathcal{M}(\Gamma_{2,4})'$ and $\mathcal{M}(\Gamma_{3,4})'$ are determined by the expansion coefficients $\widetilde{\mathbf{U}}_{2,4} \in \mathbb{C}^{\dim \mathcal{M}(\Gamma_{2,4})}$ and $\widetilde{\mathbf{U}}_{3,4} \in \mathbb{C}^{\dim \mathcal{M}(\Gamma_{3,4})}$, respectively, then

$$\langle\, \mu_{2,4;h} \mid u \,\rangle_{H^{1/2}(\Gamma_{2,4})} = \widetilde{\mathbf{U}}_{2,4}^T \int_{\Gamma_{2,4}} \mathbf{H}_{2,4} u \, d\Gamma, \tag{23c}$$

$$\langle\, \mu_{3,4;h} \mid t \,\rangle_{H^{1/2}(\Gamma_{3,4})} = \widetilde{\mathbf{U}}_{3,4}^T \int_{\Gamma_{3,4}} \mathbf{H}_{3,4} t \, d\Gamma, \tag{23d}$$

for any $u \in H^{1/2}(\Gamma_{2,4})$ and $t \in H^{1/2}(\Gamma_{3,4})$. We define the finite dimensional subspace $\mathcal{Y}_h$ of $\mathcal{Y}$ in (8b) as:

$$\mathcal{Y}_h \stackrel{\text{def}}{=} \mathcal{M}(\Gamma_{1,2})' \times \mathcal{M}(\Gamma_{2,4})' \times \mathcal{M}(\Gamma_{3,4})'. \tag{24}$$

The norm in $\mathcal{Y}_h$ is that inherited from $\mathcal{Y}$ in (10b). The reasoning above gives us the dimension of $\mathcal{Y}_h$:

$$\dim \mathcal{Y}_h = |\mathcal{B}(\Gamma_{1,2})| + |\mathcal{B}(\Gamma_{2,4})| + |\mathcal{B}(\Gamma_{3,4})|. \tag{25}$$

4.4 | Discretization

The finite-dimensional counterpart to problem (12a) is

$$\begin{aligned} &\text{Find } (\mathbf{p}_h, \boldsymbol{\lambda}_h) \in \mathcal{X}_h \times \mathcal{Y}_h \text{ such that} \\ &a(\mathbf{p}_h, \mathbf{v}_h) + b(\mathbf{v}_h, \boldsymbol{\lambda}_h) = \langle\, Q' \mid \mathbf{v}_h \,\rangle_{\mathcal{X}^\star,\mathcal{X}}, \quad \text{for any } \mathbf{v}_h \in \mathcal{X}_h, \\ &b(\mathbf{p}_h, \boldsymbol{\mu}_h) = 0, \quad \text{for any } \boldsymbol{\mu}_h \in \mathcal{Y}_h. \end{aligned} \tag{26}$$

Since the finite-dimensional spaces $\mathcal{X}_h$ and $\mathcal{Y}_h$ are isomorphic to $\mathbb{C}^{\dim \mathcal{X}_h}$ and $\mathbb{C}^{\dim \mathcal{Y}_h}$, respectively, there are vectors $\widetilde{\mathbf{P}}, \widetilde{\mathbf{V}} \in \mathbb{C}^{\dim \mathcal{X}_h}$ that uniquely determine $\mathbf{p}_h, \mathbf{v}_h \in \mathcal{X}_h$, and vectors $\widetilde{\mathbf{L}}, \widetilde{\mathbf{U}} \in \mathbb{C}^{\dim \mathcal{Y}_h}$ that uniquely determine $\boldsymbol{\lambda}_h, \boldsymbol{\mu}_h \in \mathcal{Y}_h$. Our goal is to derive a linear system in the unknowns $\widetilde{\mathbf{P}} \in \mathbb{C}^{\dim \mathcal{X}_h}$ and $\widetilde{\mathbf{L}} \in \mathbb{C}^{\dim \mathcal{Y}_h}$.

We represent $\mathbf{v}_h = (v_{1;h}, v_{2;h}, v_{3;h}, v_{4;h})$ and $\mathbf{p}_h = (p_{1;h}, p_{2;h}, p_{3;h}, p_{4;h})$, after (9a) and (18a). For each $r = 1, \cdots, 4$, we expand $v_{r;h}$ and $p_{r;h}$ as in (17a), that is, $v_{r;h} = \mathbf{H}_r^T \widetilde{\mathbf{V}}_r$ and $p_{r;h} = \mathbf{H}_r^T \widetilde{\mathbf{P}}_r$, where $\widetilde{\mathbf{V}}_r, \widetilde{\mathbf{P}}_r \in \mathbb{C}^{\dim \mathcal{M}(\Omega_r)}$. The traces of $v_{r;h}$ and of $p_{r;h}$ are expanded in accordance with (17b), that is, $\gamma_{\partial\Omega_r}(v_{r;h}) = \mathbf{T}_r^T \widetilde{\mathbf{V}}_r$ and $\gamma_{\partial\Omega_r}(p_{r;h}) = \mathbf{T}_r^T \widetilde{\mathbf{P}}_r$.

The vectors $\boldsymbol{\mu}_h$ and $\boldsymbol{\lambda}_h$ are represented as $\boldsymbol{\mu}_h = (\mu_{1,2;h}, \mu_{2,4;h}, \mu_{3,4;h})$ and $\boldsymbol{\lambda}_h = (\lambda_{1,2;h}, \lambda_{2,4;h}, \lambda_{3,4;h})$, after (9b) and (24). We assume that the coefficients in the expansion of $\mu_{1,2;h}$, $\mu_{2,4;h}$, and $\mu_{3,4;h}$ are ordered and collected into the vectors $\widetilde{\mathbf{U}}_{1,2} \in \mathbb{C}^{\dim \mathcal{M}(\Gamma_{1,2})}$, $\widetilde{\mathbf{U}}_{2,4} \in \mathbb{C}^{\dim \mathcal{M}(\Gamma_{2,4})}$, and $\widetilde{\mathbf{U}}_{3,4} \in \mathbb{C}^{\dim \mathcal{M}(\Gamma_{3,4})}$, respectively, as in Section 4.3. In the same way, the coefficients in the expansion of $\lambda_{1,2;h}$, $\lambda_{2,4;h}$, and $\lambda_{3,4;h}$ are ordered and collected into the vectors $\widetilde{\mathbf{L}}_{1,2}$, $\widetilde{\mathbf{L}}_{2,4}$, and $\widetilde{\mathbf{L}}_{3,4}$, respectively. Using (12b)-(12d), we write

$$a(\mathbf{p}_h, \mathbf{v}_h) = \widetilde{\mathbf{V}}^T \overline{\boldsymbol{A}}\, \widetilde{\mathbf{P}}, \tag{27a}$$

$$b(\mathbf{p}_h, \boldsymbol{\mu}_h) = \widetilde{\mathbf{U}}^T \overline{\boldsymbol{B}}\, \widetilde{\mathbf{P}}, \tag{27b}$$

$$b(\mathbf{v}_h, \boldsymbol{\lambda}_h) = \widetilde{\mathbf{L}}^T \overline{\boldsymbol{B}}\, \widetilde{\mathbf{V}} = \widetilde{\mathbf{V}}^T \overline{\boldsymbol{B}}^T\, \widetilde{\mathbf{L}}, \tag{27c}$$

$$\langle\, Q' \mid \mathbf{v}_h \,\rangle_{\mathcal{X}^\star,\mathcal{X}} = \widetilde{\mathbf{V}}^T \boldsymbol{F}, \tag{27d}$$

where the symmetric matrix $\overline{\boldsymbol{A}}$, the matrix $\overline{\boldsymbol{B}}$, and the vector $\boldsymbol{F}$ belong to $\mathbb{C}^{\dim \mathcal{X}_h \times \dim \mathcal{X}_h}$, $\mathbb{R}^{\dim \mathcal{Y}_h \times \dim \mathcal{X}_h}$, and $\mathbb{C}^{\dim \mathcal{X}_h}$, respectively. The coefficient vectors are recombined back into the 'parent' vectors as $\widetilde{\mathbf{V}}^T = [\widetilde{\mathbf{V}}_1^T \widetilde{\mathbf{V}}_2^T \widetilde{\mathbf{V}}_3^T \widetilde{\mathbf{V}}_4^T]$, $\widetilde{\mathbf{P}}^T = [\widetilde{\mathbf{P}}_1^T \widetilde{\mathbf{P}}_2^T \widetilde{\mathbf{P}}_3^T \widetilde{\mathbf{P}}_4^T]$, $\widetilde{\mathbf{U}}^T = [\widetilde{\mathbf{U}}_{1,2}^T \widetilde{\mathbf{U}}_{2,4}^T \widetilde{\mathbf{U}}_{3,4}^T]$, and $\widetilde{\mathbf{L}}^T = [\widetilde{\mathbf{L}}_{1,2}^T \widetilde{\mathbf{L}}_{2,4}^T \widetilde{\mathbf{L}}_{3,4}^T]$. We used (23b)-(23d) in (27b) and (27c). From (26) and (27a)-(27d), we obtain the linear system:

$$\begin{aligned} &\text{Find } (\widetilde{\mathbf{P}}, \widetilde{\mathbf{L}}) \in \mathbb{C}^{\dim \mathcal{X}_h} \times \mathbb{C}^{\dim \mathcal{Y}_h} \text{ such that} \\ &\begin{bmatrix} \overline{\boldsymbol{A}} & \overline{\boldsymbol{B}}^T \\ \overline{\boldsymbol{B}} & \mathbf{0} \end{bmatrix} \begin{bmatrix} \widetilde{\mathbf{P}} \\ \widetilde{\mathbf{L}} \end{bmatrix} = \begin{bmatrix} \boldsymbol{F} \\ \mathbf{0} \end{bmatrix}. \end{aligned} \tag{28}$$

The system in (28) above is a *saddle point linear system*. Other problems in mechanics,[1,41] and electromagnetics[16] are also associated with linear systems having this structure. Since the support of each basis function used in the construction of the meshfree spaces is small when compared to the size of the domain (see Sections 4.2 and 4.3), the matrices $\overline{\boldsymbol{A}}$ and $\overline{\boldsymbol{B}}$ in the system above are sparse. In this particular application, $\dim \mathcal{Y}_h$ is much smaller than $\dim \mathcal{X}_h$. The integrals in (12b)-(12d) can be evaluated numerically by any of the techniques routinely used in the MFS.[14-16,63,64,71] The solvability and stability of the numerical solutions derived from (26) and (28) will be discussed in Sections 6 and 7.

4.5 | The discretization length

Suppose the finite-sphere systems have been set up over all regions and all interfaces in the problem according to the principles outlined in Sections 4.2 and 4.3, respectively. For each $r = 1, \cdots, 4$, let the set $\mathbf{X}_r$ list the centers $\boldsymbol{x}_i$ of all balls in $\mathcal{B}(\Omega_r)$. Analogously, let the sets $\mathbf{X}_{1,2}$, $\mathbf{X}_{2,4}$, and $\mathbf{X}_{3,4}$ list the centers of all balls in $\mathcal{B}(\Gamma_{1,2})$, $\mathcal{B}(\Gamma_{2,4})$, and $\mathcal{B}(\Gamma_{3,4})$, respectively. We next form the union of these sets:

$$\mathbf{X} \stackrel{\text{def}}{=} \left(\bigcup_{r=1}^{4} \mathbf{X}_r \right) \bigcup (\mathbf{X}_{1,2} \cup \mathbf{X}_{2,4} \cup \mathbf{X}_{3,4}). \tag{29a}$$

The set $\mathbf{X}$ collects the centers $\boldsymbol{x}_i$ of all balls in the problem (i.e., the balls covering all regions and all interfaces). The *discretization length* h is calculated as

$$h \stackrel{\text{def}}{=} \max_{i=1,\cdots,|\mathbf{X}|} \min_{\substack{j=1,\cdots,|\mathbf{X}| \\ j \neq i}} \|\boldsymbol{x}_i - \boldsymbol{x}_j\|, \tag{29b}$$

where $|\mathbf{X}|$ is the number of elements in the set $\mathbf{X}$ (or the total number of balls in the problem).

5 | NUMERICAL EXAMPLES: SCATTERING PROBLEMS

In the examples to follow, we depart from the basic geometry given in Figure 1, and specialize the procedures to other geometries. However, these geometries are such that, in each particular instance, the assumptions made in Section 2.1 are satisfied. The solution times for the examples in Sections 5.1–5.3 are approximately 2 min, when the codes are executed on a 4 GB, 2.4 GHz laptop.

5.1 | Numerical error in the solution of a model problem

In order to study the approximation error, we construct a problem that, although not properly a scattering problem, it nevertheless possesses the same form of the scattering problems described in Sections 2.2–2.4. Consider the geometrical setting in Figure 6(A), for which $M = 1$. In this problem, we assume all quantities to be dimensionless. The material parameters of regions Ω_1 and Ω_2 are $\rho_1 = 4$ and $\rho_2 = 1$ (density), and $K_1 = 2$ and $K_2 = 1$ (bulk modulus). Consequently, the 'relative' values are $\rho_{1,rel} = 4$ and $\rho_{2,rel} = 1$, and $K_{1,rel} = 2$ and $K_{2,rel} = 1$, according to (4a) and (4b). We choose a unitary frequency, or $f = 1$. In these circumstances, the wavenumber associated with the host medium $\Omega_{M+1} = \Omega_2$ becomes $k = \omega/c = 2\pi f\sqrt{\rho_2/K_2} = 2\pi$ (see Section 2.2). The wavelength of a (hypothetical) plane wave propagating in the host medium with frequency $f = 1$ is $\lambda = 2\pi/k = 1$. Region Ω_1 is a circle with radius equal to λ, whereas the circle Γ_R has its radius adjusted to $R = 1.5\lambda$. Region Ω_1 is simply connected, and region Ω_2 (the host medium) is not simply connected, as expected (see Assumption 5 in Section 2.1). This problem has a single interface, indicated by $\Gamma_{1,2}$ in Figure 6(A), representing the interface between regions Ω_1 and Ω_2. Since the relative densities are constant, Equation (5) becomes: For $r = 1$, 2, find $p_r : \overline{\Omega}_r \longrightarrow \mathbb{C}$ such that for any $\boldsymbol{x} \in \Omega_r$,

$$\boldsymbol{\nabla}^2 p_r(\boldsymbol{x}) + k^2 \frac{\rho_{r,rel}}{K_{r,rel}} p_r(\boldsymbol{x}) = 0. \tag{30a}$$

We define the new wavenumbers $k_1 \stackrel{\text{def}}{=} k\sqrt{\rho_{1,rel}/K_{1,rel}}$ and $k_2 \stackrel{\text{def}}{=} k\sqrt{\rho_{2,rel}/K_{2,rel}}$. The boundary condition along Γ_R is chosen as: For all $\boldsymbol{x} \in \Gamma_R$,

$$\boldsymbol{\nabla} p_2(\boldsymbol{x}) \cdot \hat{\mathbf{n}}_{2,\infty}(\boldsymbol{x}) + jk_2 p_2(\boldsymbol{x}) = 1, \tag{30b}$$

where $\hat{\mathbf{n}}_{2,\infty}$ is the outward-pointing unit normal vector at $\boldsymbol{x}$. The interface conditions along $\Gamma_{1,2}$ are the same as those in (7b) and (7c). It can be verified that the solution to this problem is

$$\begin{aligned} p_1(\boldsymbol{x}) &= A_1 J_0(k_1\|\boldsymbol{x}\|), \quad \boldsymbol{x} \in \overline{\Omega}_1, \\ p_2(\boldsymbol{x}) &= A_2 J_0(k_2\|\boldsymbol{x}\|) + B_2 Y_0(k_2\|\boldsymbol{x}\|), \quad \boldsymbol{x} \in \overline{\Omega}_2, \end{aligned} \tag{30c}$$

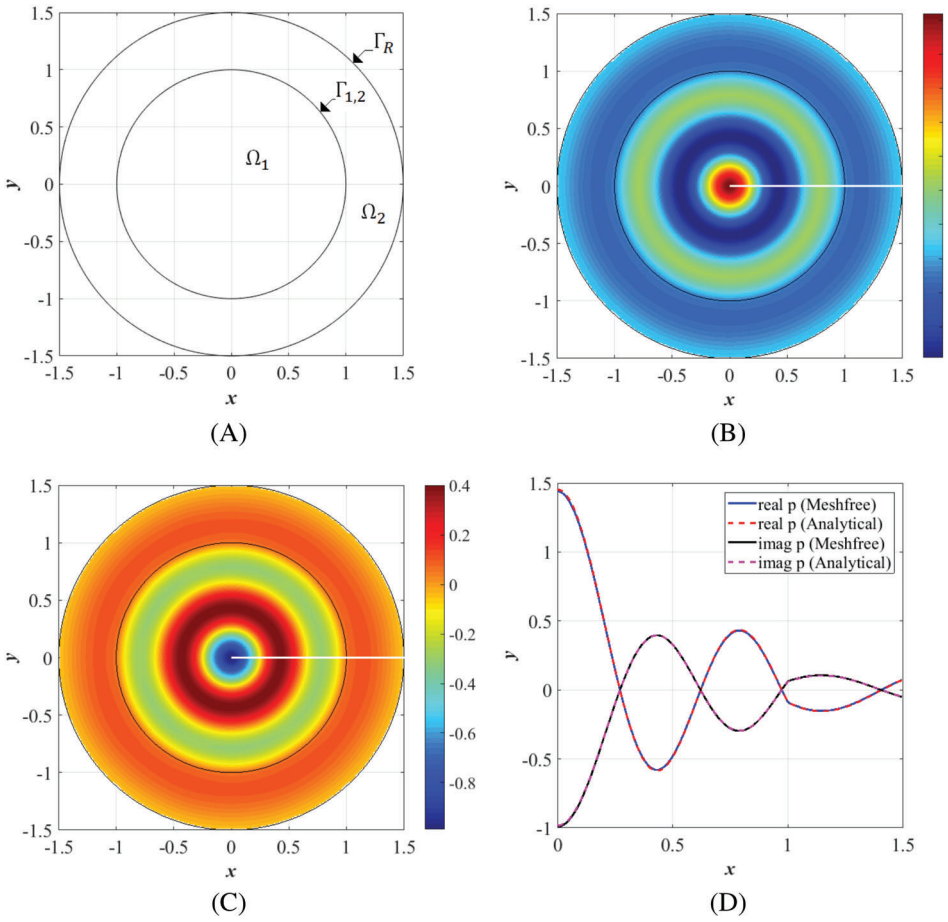

FIGURE 6 A (dimensionless) model problem for the purpose of studying the error analysis. (A) Geometry of the problem, with $M = 1$ object. (B) Real part of the solution (meshfree). (C) Imaginary part of the solution (meshfree). (D) Numerical and analytical solutions along the line segment $0 \le x \le R$, $y = 0$ (shown in white in Figure 6(B),(C))

where J_0 and Y_0 are the zero-order Bessel functions of the first and second kinds, respectively, and $\|\boldsymbol{x}\|$ is the Euclidean norm of vector $\boldsymbol{x}$. The constants A_1, A_2, and B_2 can be found by inserting (30c) into the two interface conditions along $\Gamma_{1,2}$ and into the boundary condition (30b).

In order to approximate the pressure fields p_1 and p_2 (in regions Ω_1 and Ω_2), and the Lagrange multiplier field $\lambda_{1,2}$ (along $\Gamma_{1,2}$), we employ the three finite sphere systems $\mathcal{FS}(\Omega_1)$, $\mathcal{FS}(\Omega_2)$, and $\mathcal{FS}(\Gamma_{1,2})$, respectively. The number of balls in each system is $|\mathcal{B}(\Omega_1)| = 627$ balls, $|\mathcal{B}(\Omega_2)| = 852$ balls, and $|\mathcal{B}(\Gamma_{1,2})| = 87$ balls, so that $|\mathbf{X}| = 1566$ balls (see Section 4.5). The corresponding discretization length is $h = 0.0732$, see (29b). The solution to this problem is radially symmetric, see Figure 6(B),(C). Figure 6(D) shows both the real and imaginary parts of the solution along the line $0 \le x \le R$, $y = 0$ (the white segment in Figure 6(B),(C)). The numerical solution quite closely matches the analytical solution (30c). The interface between Ω_1 and Ω_2 is at $x = 1$, and there are no oscillations close to this point (at the curve's 'knee'). Finally, we vary the number of balls in each finite sphere system so that the total number of balls in the problem $|\mathbf{X}|$ ranges from 172 to 1566. For each numerical solution $\mathbf{p}_h = (p_{1;h}, p_{2;h})$, we calculate the relative error

$$e_h \overset{\text{def}}{=} \frac{\|\mathbf{p} - \mathbf{p}_h\|_{\mathcal{X}}}{\|\mathbf{p}\|_{\mathcal{X}}} = \frac{(\|p_1 - p_{1;h}\|^2_{H^1(\Omega_1)} + \|p_2 - p_{2;h}\|^2_{H^1(\Omega_2)})^{1/2}}{(\|p_1\|^2_{H^1(\Omega_1)} + \|p_2\|^2_{H^1(\Omega_2)})^{1/2}}, \tag{30d}$$

as a function of the discretization length h, where the norm in space $\mathcal{X}$ is defined in (10a), and $\mathbf{p} = (p_1, p_2)$ is the vector collecting the analytical solutions (30c). Figure 7 shows how the error in (30d) decreases with h.

5.2 | Scattering by a kite-shaped object

We again have a single object ($M = 1$), corresponding to the kite-shaped artifact shown in Figure 8(A). The material properties in regions Ω_1 and Ω_2 are $\rho_1 = 2.80 \times 10^3$ kg/m^3 and $\rho_2 = 1 \times 10^3$ kg/m^3 (density), and $K_1 = 70 \times 10^9$ Pa and

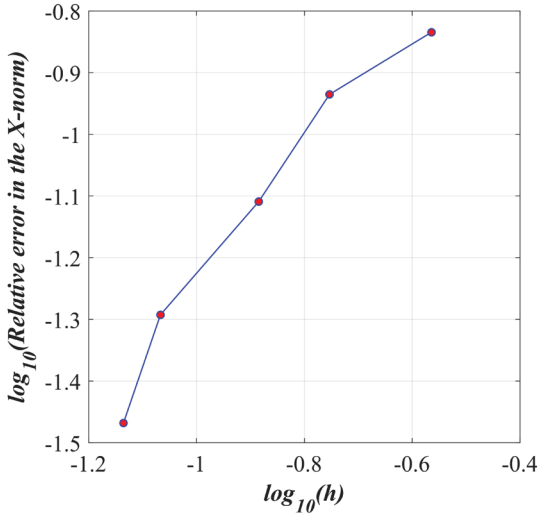

FIGURE 7 The relative error calculated in the $\mathcal{X}$-norm (10a) as a function of the discretization length h

$K_2 = 2.28\times10^9$ Pa (bulk modulus). The 'relative' values are $\rho_{1,rel} = 2.8$ and $\rho_{2,rel} = 1$, and $K_{1,rel} = 30.70$ and $K_{2,rel} = 1$, according to (4a) and (4b). Let the reference frequency be $f_0 = 5$ kHz. The reference wavenumber k_0 associated with the host medium Ω_2 is $k_0 = \omega_0/c = 2\pi f_0\sqrt{\rho_2/K_2} = 20.81$ rad/m (see Section 2.2). The reference wavelength of a (hypothetical) plane wave propagating in Ω_2 with frequency f_0 is given by $\lambda_0 = 2\pi/k_0 = 3.02\times10^{-1}$ m. Points $\boldsymbol{x} = (x_{kite}, y_{kite})$ along the contour of region Ω_1 in Figure 8(A) are described parametrically as

$$x_{kite}(\theta) = \lambda_0\frac{(\cos\theta + 0.65\cos 2\theta - 0.65)}{1.5}, \quad y_{kite}(\theta) = \lambda_0\sin\theta, \tag{31}$$

where $0 \le \theta \le 2\pi$ is the polar angle measured counterclockwise around the origin of $\mathbb{R}^2$. The radius of the outer circular boundary Γ_R is $R = 2.3\lambda_0$. Region Ω_1 is simply connected, and region Ω_2 (the host medium) is not simply connected, as expected (see Assumption 5 in Section 2.1). As in Section 5.1, this problem has a single interface, indicated by $\Gamma_{1,2}$ in Figure 8(A).

The actual incident field is given by a plane wave with frequency equal to the reference frequency, that is, $f = f_0$. The wavenumber of the problem is then given by $k = k_0$, and the direction of propagation of the plane wave is from the left to the right, that is, along the unit vector $\hat{\boldsymbol{k}} = [1, 0]$. The incident field is therefore $p^{inc}(\boldsymbol{x}) = e^{-jk\hat{\boldsymbol{k}}\cdot\boldsymbol{x}} = e^{-jkx}$ N/m^2, $\boldsymbol{x} \in \overline{\Omega}_2$.

We again set up three finite sphere systems such that $|\mathcal{B}(\Omega_1)| = 386$ balls, $|\mathcal{B}(\Omega_2)| = 2531$ balls, and $|\mathcal{B}(\Gamma_{1,2})| = 80$ balls, resulting in $|\mathbf{X}| = 2997$ balls (see Section 4.5). The modulus of the total field $\mathbf{p}_h = (p_{1;h}, p_{2;h})$, the real part, and the imaginary part are plotted throughout the computational domain in Figure 8(B)–(D), respectively. A zoom is applied to the solutions along the line segment $x_{kite}(\pi) - 0.2\lambda_0 \le x \le x_{kite}(\pi) + 0.2\lambda_0$, $y = 0$ (see Equation (31)), shown in white in Figure 8(C),(D). The real and imaginary parts of the meshfree and FEM reference solutions (for the finite element analysis we used a fine mesh of triangular quadratic Lagrangian elements) are calculated along this line segment (which crosses the interface), and are shown in Figure 8(E),(F), respectively. The agreement is very good, and the meshfree solution does not present oscillations close to the interface.

5.3 | Scattering by a cladded object

In this example the geometric setting consists of two objects ($M = 2$). It corresponds to a square column Ω_1 surrounded by a circular cladding Ω_2, shown in Figure 9(A). The structure is immersed in the host medium Ω_3. The material densities in regions Ω_1, Ω_2, and Ω_3 are $\rho_1 = 1.20$ kg/m^3, $\rho_2 = 8\times10^3$ kg/m^3, and $\rho_3 = 1\times10^3$ kg/m^3, respectively. The bulk moduli are $K_1 = 1.01\times10^5$ Pa, $K_2 = 200\times10^9$ Pa, and $K_3 = 2.28\times10^9$ Pa. The 'relative' values for the densities are $\rho_{1,rel} = 1.2\times10^{-3}$, $\rho_{2,rel} = 8$, and $\rho_{3,rel} = 1$, whereas the 'relative' values for the bulk moduli are $K_{1,rel} = 4.43\times10^{-5}$, $K_{2,rel} = 87.72$, and $K_{3,rel} = 1$, according to (4a) and (4b). The reference frequency is chosen as $f_0 = 1$ kHz, and consequently the reference

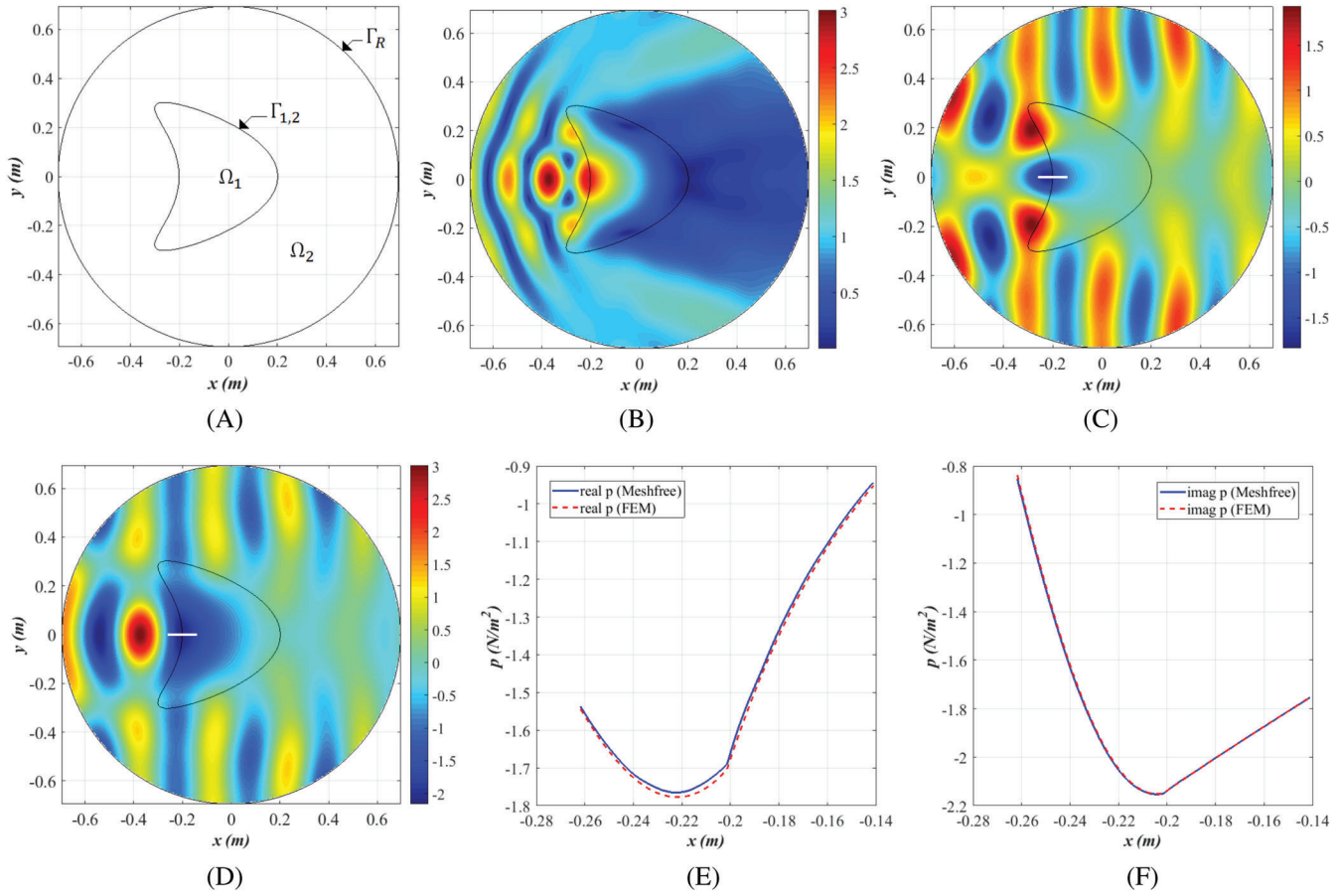

FIGURE 8 Scattering by a kite-shaped object. (A) Geometry of the problem. (B) The modulus of the meshfree solution throughout the computational domain. (C) Real part of the meshfree solution. (D) Imaginary part of the meshfree solution. (E) Real part of meshfree and FEM solutions along the segment $x_{kite}(\pi) - 0.2\lambda_0 \leq x \leq x_{kite}(\pi) + 0.2\lambda_0$, $y = 0$ (shown in white in Figure 8(C)). (F) Imaginary part of meshfree and FEM solutions along the same segment (shown in white in Figure 8(D))

wavenumber k_0 associated with the host medium Ω_3 is $k_0 = \omega_0/c = 2\pi f_0\sqrt{\rho_3/K_3} = 4.16$ rad/m (see Section 2.2). The reference wavelength of a (hypothetical) plane wave propagating in Ω_3 with frequency f_0 is given by $\lambda_0 = 2\pi/k_0 = 1.51$ m. The side of the square column is λ_0, and the radius of the circular cladding is also λ_0, see Figure 9(A). The radius of the outer circular boundary Γ_R is $R = 1.75\lambda_0$. Region Ω_1 is simply connected, whereas regions Ω_2 and Ω_3 are not simply connected. This problem has two interfaces, indicated by $\Gamma_{1,2}$ and $\Gamma_{2,3}$ in Figure 9(A), representing the interfaces between regions Ω_1 and Ω_2, and between regions Ω_2 and Ω_3, respectively.

The actual incident field is given by a plane wave with frequency equal to three times the reference frequency, that is, $f = 3f_0$. The wavenumber of the problem is then given by $k = \omega/c = 2\pi f\sqrt{\rho_3/K_3} = 12.48$ rad/m (see Section 2.2). The direction of propagation of the plane wave is from the left to the right, that is, along the unit vector $\widehat{\boldsymbol{k}} = [1, 0]$. The incident field is therefore $p^{inc}(\boldsymbol{x}) = e^{-jk\widehat{\boldsymbol{k}}\cdot\boldsymbol{x}} = e^{-jkx}$ N/m^2, $\boldsymbol{x} \in \overline{\Omega}_3$.

In order to approximate the pressure fields p_1, p_2, and p_3 (in regions Ω_1, Ω_2, and Ω_3), and the Lagrange multiplier fields $\lambda_{1,2}$ (along $\Gamma_{1,2}$) and $\lambda_{2,3}$ (along $\Gamma_{2,3}$), we employ the five finite sphere systems $\mathcal{FS}(\Omega_1)$, $\mathcal{FS}(\Omega_2)$, $\mathcal{FS}(\Omega_3)$, $\mathcal{FS}(\Gamma_{1,2})$, and $\mathcal{FS}(\Gamma_{2,3})$, respectively. The number of balls in each system is $|\mathcal{B}(\Omega_1)| = 192$ balls, $|\mathcal{B}(\Omega_2)| = 417$ balls, $|\mathcal{B}(\Omega_3)| = 1195$ balls, $|\mathcal{B}(\Gamma_{1,2})| = 48$ balls, and $|\mathcal{B}(\Gamma_{2,3})| = 81$ balls, so that $|\mathbf{X}| = 1933$ balls (see Section 4.5). The modulus, the real part, and the imaginary part of the total field $\mathbf{p}_h = (p_{1;h}, p_{2;h}, p_{3;h})$ are plotted throughout the computational domain in Figure 9(B)–(D), respectively. A zoom is applied to the solutions along the line segment $-1.25\lambda_0 \leq x \leq -0.25\lambda_0$, $y = 0$, shown in white in Figure 9(C),(D). This segment crosses the two interfaces $\Gamma_{1,2}$ and $\Gamma_{2,3}$. We calculate the real and imaginary parts of the meshfree and FEM reference solutions (using a fine mesh of triangular quadratic Lagrangian elements) along this segment. They agree with each other, as shown in Figure 9(E),(F), and again there are no oscillations close to the interfaces in the meshfreesolutions.

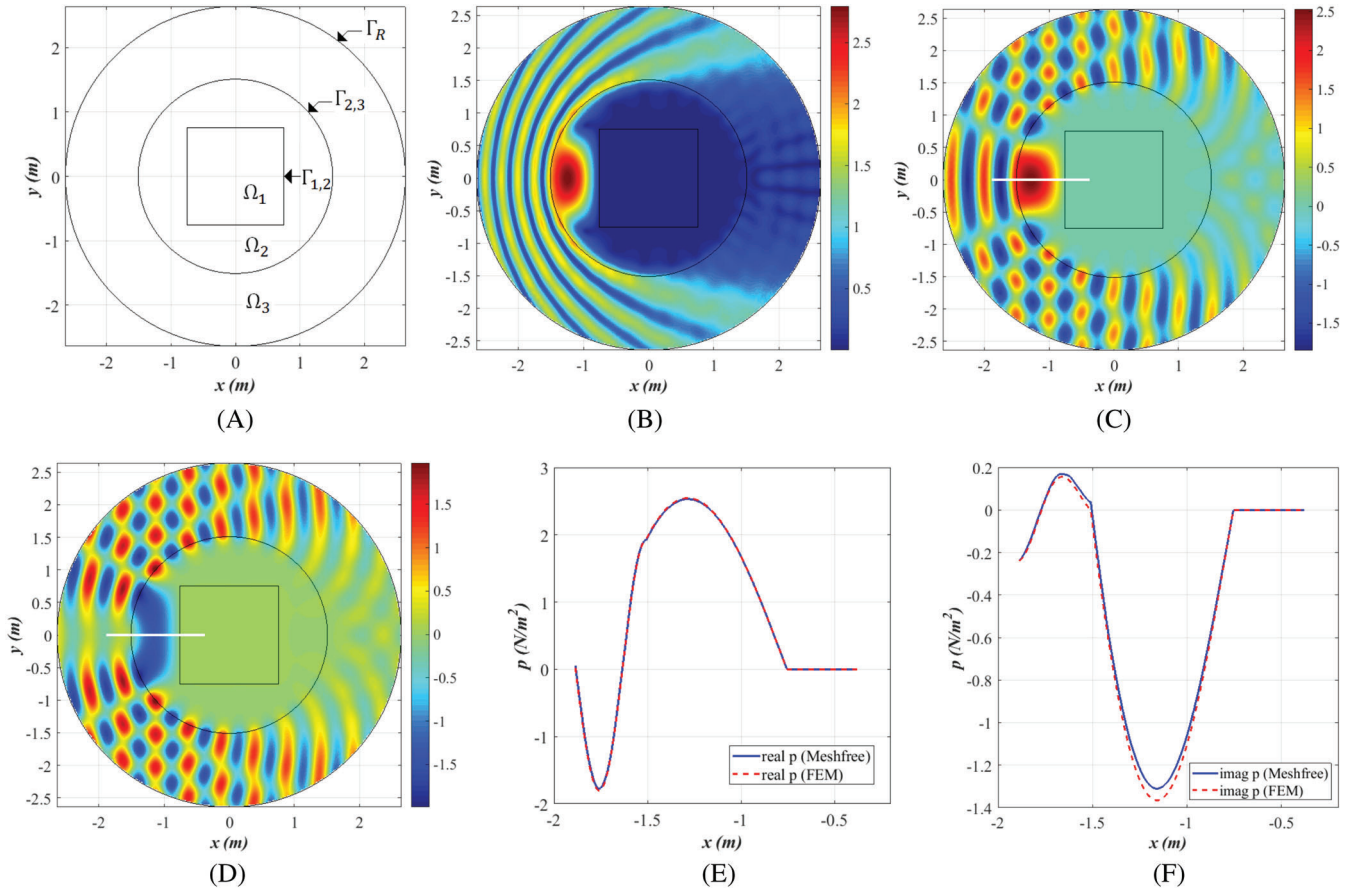

FIGURE 9 Scattering by a square column surrounded by a circular cladding. (A) Geometry of the problem. (B) The modulus of the meshfree solution throughout the computational domain. (C) Real part of the meshfree solution. (D) Imaginary part of the meshfree solution. (E) Real part of meshfree and FEM solutions along the line segment $-1.25\lambda_0 \leq x \leq -0.25\lambda_0, y = 0$ (shown in white in Figure 9(C)). (F) Imaginary part of meshfree and FEM solutions along the same segment (shown in white in Figure 9(D))

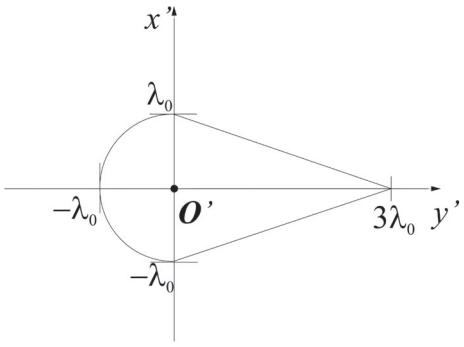

FIGURE 10 Dimensions of an object centered at the origin $\boldsymbol{O'}$

5.4 | Scattering by a group of objects

In this example, the geometric setting consists of three objects ($M = 3$). They are 'torpedo-like' in form, as shown in Figure 10. These objects occupy the regions corresponding to Ω_1, Ω_2, and Ω_3 in Figure 11(A), and are immersed in the host medium Ω_4. The material densities in the problem are $\rho_1 = \rho_2 = \rho_3 = 8 \times 10^3$ kg/m^3, and $\rho_4 = 1 \times 10^3$ kg/m^3. The bulk moduli are given by $K_1 = K_2 = K_3 = 200 \times 10^9$ Pa, and $K_4 = 2.28 \times 10^9$ Pa. The 'relative' values for the densities are $\rho_{1,rel} = \rho_{2,rel} = \rho_{3,rel} = 8$, and $\rho_{4,rel} = 1$, whereas the 'relative' values for the bulk moduli are $K_{1,rel} = K_{2,rel} = K_{3,rel} = 87.72$, and $K_{4,rel} = 1$, according to (4a) and (4b).

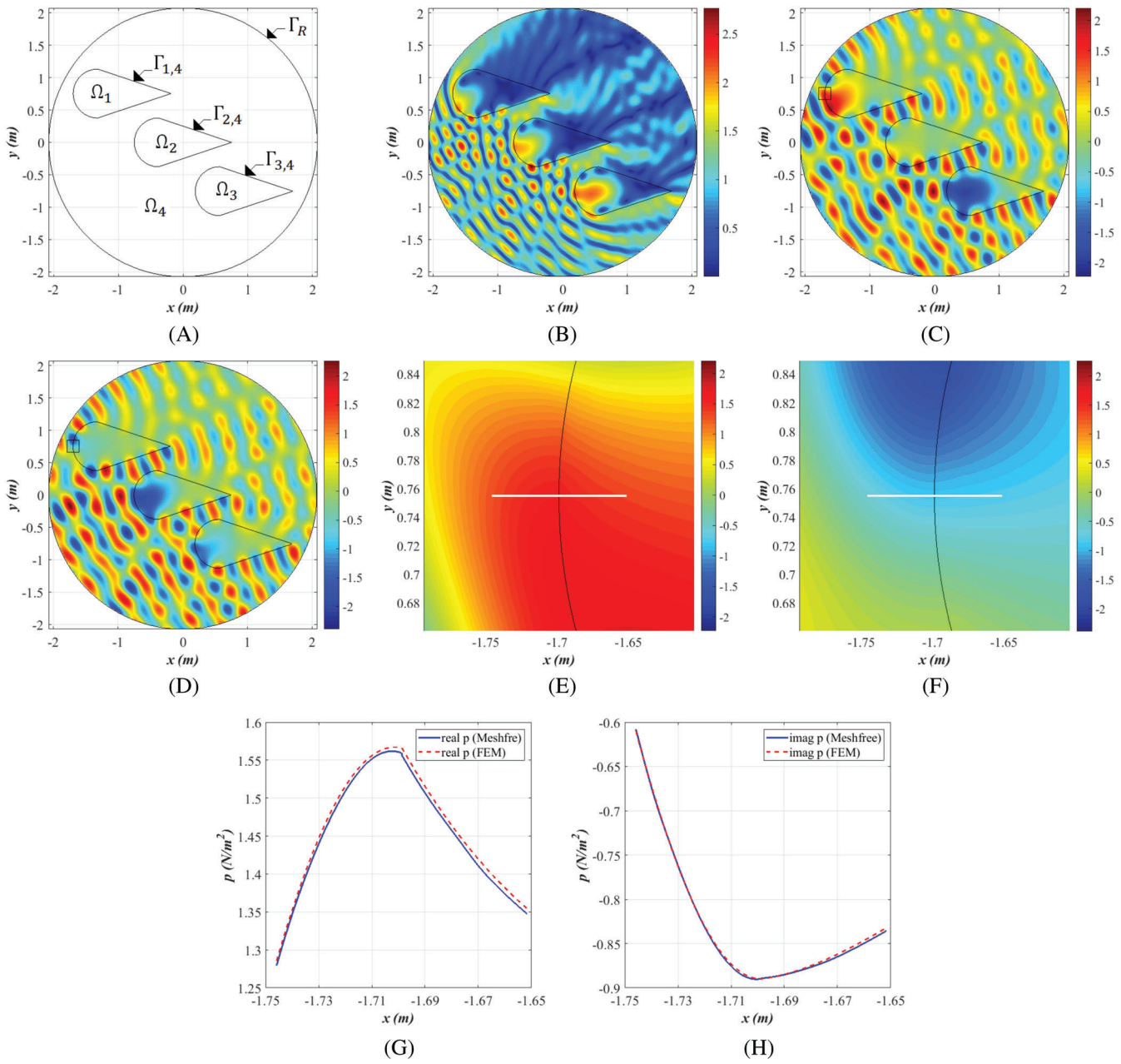

FIGURE 11 Scattering by a group of three objects. (A) Geometry of the problem. (B) The modulus of the meshfree solution throughout the computational domain. (C) Real part of the meshfree solution. (D) Imaginary part of the meshfree solution. (E) Real part of the meshfree solution in the small square region shown in (C). (F) Imaginary part of the meshfree solution in the small square region shown in (D). (G) Real part of meshfree and FEM solutions along the segment $-4.625\lambda_0 \leq x \leq -4.375\lambda_0, y = 2\lambda_0$ (shown in white in (E)). (H) Imaginary part of meshfree and FEM solutions along the same segment (shown in white in (F))

We choose a reference frequency of $f_0 = 4$ kHz, and the reference wavenumber k_0 associated with the host medium Ω_4 is $k_0 = \omega_0/c = 2\pi f_0\sqrt{\rho_4/K_4} = 16.65$ rad/m (see Section 2.2). The reference wavelength of a (hypothetical) plane wave propagating in Ω_4 with frequency f_0 is given by $\lambda_0 = 2\pi/k_0 = 0.37$ m. Each object is formed by a semicircle of radius λ_0 connected to an isosceles triangle with base $2\lambda_0$ (the diameter of the semicircle) and height $3\lambda_0$, see Figure 10. Figure 10 shows a single object drawn in a relative coordinate system $x'y'$ whose origin $\boldsymbol{O}'$ coincides with the center of the semicircle. In the absolute coordinate system xy (in which the problem is posed), object 1 is located in such a way that $\boldsymbol{O}' = (-3.5\lambda_0, 2\lambda_0)$, object 2 is such that $\boldsymbol{O}' = (-\lambda_0, 0)$, and object 3 is such that $\boldsymbol{O}' = (1.5\lambda_0, -2\lambda_0)$, see Figure 11(A). The radius of the outer circular boundary Γ_R is $R = 5.5\lambda_0$. Regions Ω_1, Ω_2, and Ω_3 are simply connected, whereas region

Ω_4 (the host medium) is not simply connected (see Figure 11(A)). This problem has three interfaces, indicated by $\Gamma_{1,4}$, $\Gamma_{2,4}$, and $\Gamma_{3,4}$ in Figure 11(A), which represent the interfaces between regions Ω_1 and Ω_4, between regions Ω_2 and Ω_4, and between regions Ω_3 and Ω_4, respectively.

The actual incident field is given by a plane wave with frequency equal to the reference frequency, that is, $f = f_0$, so that the wavenumber of the problem is given by $k = k_0 = 16.65$ rad/m (see Section 2.2). The incident plane wave propagates in the direction of the unit vector $\widehat{\boldsymbol{k}} = [\cos 30° \sin 30°] = [\sqrt{3}/2, 1/2]$, and the expression for the incident field is therefore given by $p^{inc}(\boldsymbol{x}) = e^{-jk\widehat{\boldsymbol{k}}\cdot\boldsymbol{x}} = e^{-jk(\sqrt{3}x+y)/2}$ N/m^2, $\boldsymbol{x} \in \overline{\Omega}_4$.

In order to approximate the pressure fields p_1, p_2, p_3, and p_4 (in regions Ω_1, Ω_2, Ω_3, and Ω_4), and the Lagrange multiplier fields $\lambda_{1,4}$ (along $\Gamma_{1,4}$), $\lambda_{2,4}$ (along $\Gamma_{2,4}$), and $\lambda_{3,4}$ (along $\Gamma_{3,4}$), we use the seven finite sphere systems $\mathcal{FS}(\Omega_1)$, $\mathcal{FS}(\Omega_2)$, $\mathcal{FS}(\Omega_3)$, $\mathcal{FS}(\Omega_4)$, $\mathcal{FS}(\Gamma_{1,4})$, $\mathcal{FS}(\Gamma_{2,4})$, and $\mathcal{FS}(\Gamma_{3,4})$, respectively. The number of balls in each system is $|\mathcal{B}(\Omega_1)| = 487$ balls, $|\mathcal{B}(\Omega_2)| = 470$ balls, $|\mathcal{B}(\Omega_3)| = 474$ balls, $|\mathcal{B}(\Omega_4)| = 8011$ balls, and $|\mathcal{B}(\Gamma_{1,4})| = |\mathcal{B}(\Gamma_{2,4})| = |\mathcal{B}(\Gamma_{3,4})| = 90$ balls, so that $|\mathbf{X}| = 9712$ balls (see Section 4.5). The modulus, the real part, and the imaginary part of the total field $\mathbf{p}_h = (p_{1;h}, p_{2;h}, p_{3;h}, p_{4;h})$ are plotted throughout the computational domain in Figure 11(B)–(D), respectively. We examine the fields closely in a small box placed at the front end of object 1 (see Figure 11(C),(D)). This square box is centered at the point $(-4.5\lambda_0, 2\lambda_0)$ (the front end of object 1), and its side is $\lambda_0/2$ in length, so that it corresponds to the region $-4.75\lambda_0 \le x \le -4.25\lambda_0$, $1.75\lambda_0 \le y \le 2.25\lambda_0$. A zoom is applied to this region, and the fields are shown in Figure 11(E),(F). The interface $\Gamma_{1,4}$ cuts through this box, and the line segment described by $-4.625\lambda_0 \le x \le -4.375\lambda_0$, $y = 2\lambda_0$, by its turn, crosses the interface $\Gamma_{1,4}$ as illustrated in Figure 11(E),(F). This segment is shown in white. Meshfree and FEM solutions (using a fine mesh of triangular quadratic Lagrangian elements) are calculated along this line segment, and the results are given in Figure 11(G),(H). Again, the meshfree solutions are able to reproduce the discontinuity in the gradients, without oscillations close to the interface.

6 | THE INF-SUP CONDITIONS

The well-posedness of problems (12a) and (26) is described by the classical theory of mixed (or hybrid) formulations.[1,2,39-41,82,85,86] When the results of this theory are specialized to the scattering problems studied in this work, it can be shown that the well-posedness of the finite-dimensional problem (26) is governed by the following theorem:

Theorem 1. Consider the finite-dimensional subspaces $\mathcal{X}_h \subset \mathcal{X}$ and $\mathcal{Y}_h \subset \mathcal{Y}$. Let $a : \mathcal{X} \times \mathcal{X} \longrightarrow \mathbb{C}$ and $b : \mathcal{X} \times \mathcal{Y} \longrightarrow \mathbb{C}$ be the two bounded bilinear forms introduced in (12b) and (12c), respectively. The finite-dimensional saddle-point problem (26) is well-posed (i.e., its solution exists, is unique, and depends continuously on the data) if and only if the following two conditions are satisfied:

1. There is a constant $\alpha_h > 0$ such that $\inf\limits_{\substack{\mathbf{w}_h \in \ker B_h \\ \mathbf{w}_h \neq \mathbf{0}}} \sup\limits_{\substack{\mathbf{v}_h \in \ker B_h \\ \mathbf{v}_h \neq \mathbf{0}}} \dfrac{|a(\mathbf{w}_h, \mathbf{v}_h)|}{\|\mathbf{w}_h\|_{\mathcal{X}} \|\mathbf{v}_h\|_{\mathcal{X}}} \ge \alpha_h,$
2. There is a constant $\beta_h > 0$ such that $\inf\limits_{\substack{\boldsymbol{\mu}_h \in \mathcal{Y}_h \\ \boldsymbol{\mu}_h \neq \mathbf{0}}} \sup\limits_{\substack{\mathbf{v}_h \in \mathcal{X}_h \\ \mathbf{v}_h \neq \mathbf{0}}} \dfrac{|b(\mathbf{v}_h, \boldsymbol{\mu}_h)|}{\|\boldsymbol{\mu}_h\|_{\mathcal{Y}} \|\mathbf{v}_h\|_{\mathcal{X}}} \ge \beta_h,$

where the spaces $\mathcal{X}$, $\mathcal{Y}$, $\mathcal{X}_h$, and $\mathcal{Y}_h$ are given in (8a), (8b), (18a), and (24), respectively. These are referred to as the (discrete) *inf-sup conditions*. ■

In (32a), B_h is the operator $B_h : \mathcal{X}_h \longrightarrow \mathcal{Y}_h^\star$, which is defined as: For any $(\mathbf{v}_h \boldsymbol{\mu}_h) \in \mathcal{X}_h \times \mathcal{Y}_h$,

$$\langle\, B_h(\mathbf{v}_h) \mid \boldsymbol{\mu}_h \,\rangle_{\mathcal{Y}_h^\star, \mathcal{Y}_h} \stackrel{\text{def}}{=} b(\mathbf{v}_h, \boldsymbol{\mu}_h). \tag{33}$$

The kernel (or nullspace) of B_h is denoted by $\ker B_h$, and $\mathcal{Y}_h^\star$ is the dual space of $\mathcal{Y}_h$.[40,41,80,82] These conditions are discussed in detail in another paper.[72] In that work, we touch on subjects like the non-coercivity (or non-ellipticity[87]) of the bilinear form a derived from the Helmholtz equation,[88] and also on ways to overcome the difficulty of dealing with norms in the fractional Sobolev space $H^{-1/2}$, which are embedded in the norm of the space $\mathcal{Y}$, according to (8b), (10b), and (11b).

Then we finally derive[72] stronger and simplified inf-sup conditions, in which only real-valued numbers (i.e., real-valued vectors and matrices) are used (we no longer use complex numbers). These are given by:

$$\text{1. There is a constant } \alpha_h > 0 \text{ such that } \inf_{\substack{\widetilde{\mathfrak{w}}\in\mathbb{R}^{2K}\\ \widetilde{\mathfrak{w}}\neq\mathbf{0}}} \sup_{\substack{\widetilde{\mathfrak{v}}\in\mathbb{R}^{2K}\\ \widetilde{\mathfrak{v}}\neq\mathbf{0}}} \frac{\widetilde{\mathfrak{w}}^T\overline{\mathbb{A}}\,\widetilde{\mathfrak{v}}}{\sqrt{\widetilde{\mathfrak{w}}^T\overline{\mathbb{D}}\,\widetilde{\mathfrak{w}}}\sqrt{\widetilde{\mathfrak{v}}^T\overline{\mathbb{D}}\,\widetilde{\mathfrak{v}}}} \geq \alpha_h, \tag{34a}$$

$$\text{2. There is a constant } \beta_h > 0 \text{ such that } \inf_{\substack{\widetilde{\mathfrak{u}}\in\mathbb{R}^{2\dim\mathcal{Y}_h}\\ \widetilde{\mathfrak{u}}\neq\mathbf{0}}} \sup_{\substack{\widetilde{\mathfrak{v}}\in\mathbb{R}^{2\dim\mathcal{X}_h}\\ \widetilde{\mathfrak{v}}\neq\mathbf{0}}} \frac{\widetilde{\mathfrak{u}}^T\,\overline{\mathbb{B}}\,\widetilde{\mathfrak{v}}}{\sqrt{\widetilde{\mathfrak{u}}^T\overline{\mathbb{M}}\,\widetilde{\mathfrak{u}}}\sqrt{\widetilde{\mathfrak{v}}^T\overline{\mathbb{X}}\,\widetilde{\mathfrak{v}}}} \geq \beta_h, \tag{34b}$$

where K is the dimension of B_h.[72] We show[72] that condition (34a) is sufficient to imply condition (32a), that is, if (34a) holds true, then (32a) also holds true. In the same way, (34b) is sufficient to imply (32b). These new conditions form the basis of the inf-sup testing procedure, described in Section 7. The matrices $\overline{\mathbb{A}}$, $\overline{\mathbb{D}}$, $\overline{\mathbb{B}}$, $\overline{\mathbb{M}}$, and $\overline{\mathbb{X}}$ are given by

$$\overline{\mathbb{A}} \overset{\text{def}}{=} \text{Re}\{\overline{\mathbf{J}}_K^T\overline{\boldsymbol{\Psi}}^T\overline{\boldsymbol{A}}\,\overline{\boldsymbol{\Psi}}\,\overline{\mathbf{J}}_K\}, \tag{35a}$$

$$\overline{\mathbb{D}} \overset{\text{def}}{=} \text{Re}\{\overline{\mathbf{J}}_K^\dagger\overline{\boldsymbol{\Psi}}^\dagger\overline{\boldsymbol{S}}\,\overline{\boldsymbol{\Psi}}\,\overline{\mathbf{J}}_K\}, \tag{35b}$$

$$\overline{\mathbb{B}} \overset{\text{def}}{=} \text{Re}\{\overline{\mathbf{J}}_{\dim\mathcal{Y}_h}^T\overline{\boldsymbol{B}}\,\overline{\mathbf{J}}_{\dim\mathcal{X}_h}\}, \tag{35c}$$

$$\overline{\mathbb{M}} \overset{\text{def}}{=} \text{Re}\{\overline{\mathbf{J}}_{\dim\mathcal{Y}_h}^\dagger\overline{\boldsymbol{N}}^T\overline{\boldsymbol{Q}}^{-1}\overline{\boldsymbol{N}}\,\overline{\mathbf{J}}_{\dim\mathcal{Y}_h}\}, \tag{35d}$$

$$\overline{\mathbb{X}} \overset{\text{def}}{=} \text{Re}\{\overline{\mathbf{J}}_{\dim\mathcal{X}_h}^\dagger\overline{\boldsymbol{S}}\,\overline{\mathbf{J}}_{\dim\mathcal{X}_h}\}, \tag{35e}$$

where the matrices $\overline{\boldsymbol{A}}$ and $\overline{\boldsymbol{B}}$ in (35a) and (35c) are the same as those in (27a) and (27b), respectively. The matrices $\overline{\mathbb{A}}$, $\overline{\mathbb{D}}$, $\overline{\mathbb{M}}$, and $\overline{\mathbb{X}}$ are symmetric. Specifically, the matrices $\overline{\mathbb{D}}$, $\overline{\mathbb{M}}$, and $\overline{\mathbb{X}}$ are used in appropriate norms.[72] The symbols $\overline{\mathbf{J}}_K$, $\overline{\boldsymbol{\Psi}}$, $\overline{\boldsymbol{S}}$, $\overline{\mathbf{J}}_{\dim\mathcal{X}_h}$, $\overline{\mathbf{J}}_{\dim\mathcal{Y}_h}$, $\overline{\boldsymbol{N}}$, and $\overline{\boldsymbol{Q}}$ denote other auxiliary matrices.[72]

7 | INF-SUP TESTING

7.1 | First inf-sup condition

In order to evaluate if condition (34a) holds, we first verify if $\ker\overline{\mathbb{A}}^T = \{\mathbf{0}\}$.

Case 1. $\ker\overline{\mathbb{A}}^T \neq \{\mathbf{0}\}$. This implies that there are vectors $\widetilde{\mathfrak{w}} \in \mathbb{R}^{2K}$ such that $\widetilde{\mathfrak{w}} \neq \mathbf{0}$ and $\overline{\mathbb{A}}^T\widetilde{\mathfrak{w}} = \mathbf{0}$. If we pick up one of these vectors $\widetilde{\mathfrak{w}}$, it follows that for any vector $\widetilde{\mathfrak{v}} \in \mathbb{R}^{2K}$, it is the case that $\widetilde{\mathfrak{w}}^T\overline{\mathbb{A}}\,\widetilde{\mathfrak{v}} = \widetilde{\mathfrak{v}}^T\overline{\mathbb{A}}^T\,\widetilde{\mathfrak{w}} = 0$, and (34a) cannot be satisfied.

Case 2. $\ker\overline{\mathbb{A}}^T = \{\mathbf{0}\}$. In this case, it can be proven[40,41] (since we are left with real-valued matrices and vectors) that

$$\inf_{\substack{\widetilde{\mathfrak{w}}\in\mathbb{R}^{2K}\\ \widetilde{\mathfrak{w}}\neq\mathbf{0}}} \sup_{\substack{\widetilde{\mathfrak{v}}\in\mathbb{R}^{2K}\\ \widetilde{\mathfrak{v}}\neq\mathbf{0}}} \frac{\widetilde{\mathfrak{w}}^T\overline{\mathbb{A}}\,\widetilde{\mathfrak{v}}}{\sqrt{\widetilde{\mathfrak{w}}^T\overline{\mathbb{D}}\,\widetilde{\mathfrak{w}}}\sqrt{\widetilde{\mathfrak{v}}^T\overline{\mathbb{D}}\,\widetilde{\mathfrak{v}}}} = \sqrt{\sigma_{\min}(h)}, \tag{36a}$$

where $\sigma_{\min}(h)$ is the smallest eigenvalue in the problem:

$$\overline{\mathbb{A}}\,\overline{\mathbb{D}}^{-1}\overline{\mathbb{A}}^T\widetilde{\mathfrak{w}}_i = \sigma_i\overline{\mathbb{D}}\,\widetilde{\mathfrak{w}}_i. \tag{36b}$$

This smallest eigenvalue depends on the matrices $\overline{\mathbb{A}}$ and $\overline{\mathbb{D}}$, constructed with basis functions from spaces $\mathcal{X}_h$ and $\mathcal{Y}_h$ in (18a) and (24), respectively, which are characterized by the discretization length h (29b). So $\sigma_{\min}$ can be 'indexed' by h, and we write $\sigma_{\min}(h)$. Therefore, according to (36a), condition (34a) is satisfied if $\sqrt{\sigma_{\min}(h)} > 0$, that is, the choice $\alpha_h = \sqrt{\sigma_{\min}(h)}$ satisfies (34a).

7.2 | Second inf-sup condition

Condition (34b) is verified likewise, that is, we first check if $\ker \overline{\mathbb{B}}^T = \{\mathbf{0}\}$.

Case 1. $\ker \overline{\mathbb{B}}^T \neq \{\mathbf{0}\}$. This implies that there are vectors $\widetilde{\mathbf{u}} \in \mathbb{R}^{2\dim \mathcal{Y}_h}$ such that $\widetilde{\mathbf{u}} \neq \mathbf{0}$ and $\overline{\mathbb{B}}^T \widetilde{\mathbf{u}} = \mathbf{0}$. If we pick up one of these vectors $\widetilde{\mathbf{u}}$, it follows that for any vector $\widetilde{\mathbf{v}} \in \mathbb{R}^{2\dim \mathcal{X}_h}$, it is the case that $\widetilde{\mathbf{u}}^T \overline{\mathbb{B}}\, \widetilde{\mathbf{v}} = \widetilde{\mathbf{v}}^T \overline{\mathbb{B}}^T \widetilde{\mathbf{u}} = 0$, and (34b) cannot be satisfied.

Case 2. $\ker \overline{\mathbb{B}}^T = \{\mathbf{0}\}$. In this case, it can be shown that

$$\inf_{\substack{\widetilde{\mathbf{u}} \in \mathbb{R}^{2\dim \mathcal{Y}_h} \\ \widetilde{\mathbf{u}} \neq \mathbf{0}}} \sup_{\substack{\widetilde{\mathbf{v}} \in \mathbb{R}^{2\dim \mathcal{X}_h} \\ \widetilde{\mathbf{v}} \neq \mathbf{0}}} \frac{\widetilde{\mathbf{u}}^T \overline{\mathbb{B}}\, \widetilde{\mathbf{v}}}{\sqrt{\widetilde{\mathbf{u}}^T \overline{\mathbb{M}}\, \widetilde{\mathbf{u}}}\, \sqrt{\widetilde{\mathbf{v}}^T \overline{\mathbb{X}}\, \widetilde{\mathbf{v}}}} = \sqrt{\tau_{\min}(h)}, \tag{37a}$$

where $\tau_{\min}(h)$ is the smallest eigenvalue in the problem:

$$\overline{\mathbb{B}}\, \overline{\mathbb{X}}^{-1} \overline{\mathbb{B}}^T \widetilde{\mathbf{u}}_i = \tau_i \overline{\mathbb{M}}\, \widetilde{\mathbf{u}}_i. \tag{37b}$$

According to (37a), condition (34b) is satisfied if $\sqrt{\tau_{\min}(h)} > 0$, that is, the choice $\beta_h = \sqrt{\tau_{\min}(h)}$ satisfies (34b).

7.3 | Stability analysis and testing

In the stability analysis, we are concerned with the ability of the discrete problems to retain their well-posedness as the finite-dimensional subspaces $\mathcal{X}_h$ and $\mathcal{Y}_h$ are successively refined, or as the discretization length h becomes successively smaller.[1,39,40] In order for the discrete problem (26) to retain its well-posedness, four hypotheses must be satisfied. They are:

1. $\ker \overline{\mathbb{A}}^T = \{\mathbf{0}\}$, for all $h > 0$,
2. $\ker \overline{\mathbb{B}}^T = \{\mathbf{0}\}$, for all $h > 0$.

These two hypotheses come from Case 2 in Sections 7.1 and 7.2, respectively. If they hold true, the inf-sup values $\sqrt{\sigma_{\min}(h)}$ and $\sqrt{\tau_{\min}(h)}$ in (36a) and (37a) can be calculated for any h. The third and fourth hypotheses are:

3. $\inf\limits_{h>0} \sqrt{\sigma_{\min}(h)} > 0$,
4. $\inf\limits_{h>0} \sqrt{\tau_{\min}(h)} > 0$.

The last two hypotheses guarantee that the inf-sup values do not approach zero as h becomes smaller.

From a practical viewpoint, it is unreasonable to directly verify these four hypotheses for all $h > 0$, because the number of tests to be performed is infinite. In the practical stability testing, we do not prove that the third and fourth hypotheses are satisfied, but evaluate the likelihood that they will not be violated.[1] This is accomplished by verifying the four hypotheses above for a finite sequence of K_{test} values for h. If it is the case that the kernels of $\overline{\mathbb{A}}^T$ and $\overline{\mathbb{B}}^T$ are always zero, it suffices to investigate the smallest eigenvalues $\sigma_{\min}(h)$ and $\tau_{\min}(h)$ until a trend is detected. Ideally, these terms should 'lock', or stabilize at a given value greater than zero, which allows us to conclude that the third and fourth hypotheses are unlikely to be violated. In this case, we say that the inf-sup test has been passed. Experience shows that a choice of K_{test} between 5 and 10 is sufficient to reveal the trend.

The first ideas concerning the practical stability testing were introduced by Chapelle and Bathe,[89] and then discussed and successfully applied in later works[69,90-95] in the context of FEMs. We make the following remark: According to (35a), the matrix $\overline{\mathbb{A}}$ depends on the matrix $\overline{\boldsymbol{A}}$. The matrix $\overline{\boldsymbol{A}}$ in turn depends on the wavenumber k, since it comes from the discretization of the bilinear form a, see (12b) and (27a). But $k = \omega/c$, where $\omega = 2\pi f$ and c is a constant (the speed of sound in the host medium, see Section 2.2). In this way, $\overline{\mathbb{A}}$ depends on the frequency f of the incident field. Therefore,

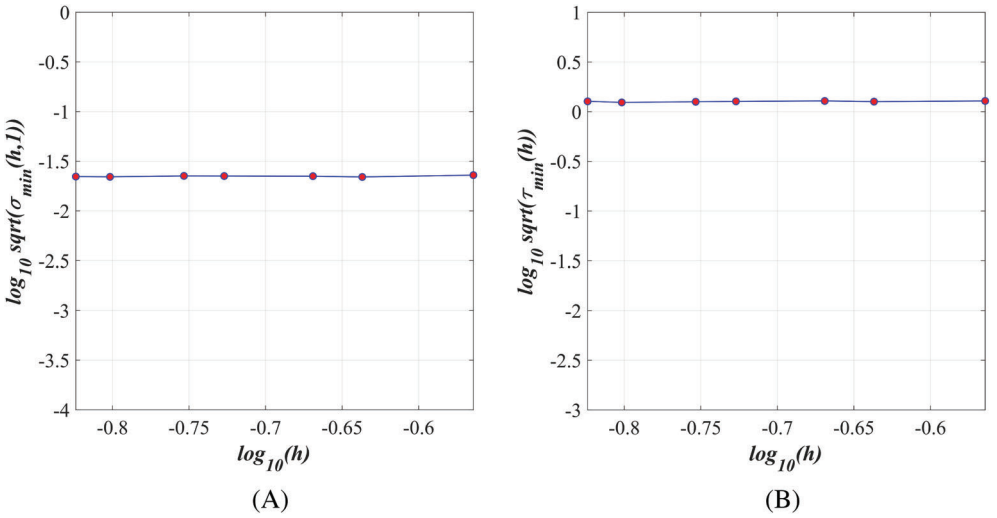

FIGURE 12 The inf-sup values for the model problem solved in Section 5.1. (A) First inf-sup condition, $\log_{10}\sqrt{\sigma_{\min}(h,1)}$ as a function of $\log_{10}h$. (B) Second inf-sup condition, $\log_{10}\sqrt{\tau_{\min}(h)}$ as a function of $\log_{10}h$

the smallest eigenvalue $\sigma_{\min}$ in (36b) also depends on f. We write $\sigma_{\min}(h,f)$ in order to show the dependence of $\sigma_{\min}$ on h and f. These testing procedures will now be applied to the four examples studied in Section 5.

8 | NUMERICAL EXAMPLES: THE INF-SUP TEST

We report that in all four examples examined in Section 5, the matrices $\overline{\mathbb{A}}^T$ and $\overline{\mathbb{B}}^T$ have only the zero vector in their kernels, for each one of the K_{test} times the tests were performed. In this way, the first and second hypotheses from Section 7 have been verified. The next subsections are devoted to testing the third and fourth hypotheses.

8.1 | Solution of a model problem (Section 5.1)

In this example, we use $K_{test} = 7$. The sequence of finite sphere systems is such that the number of balls over Ω_1 varies from 57 to 164, the number of balls over Ω_2 varies from 90 to 240, and the number of balls over $\Gamma_{1,2}$ varies from 25 to 43.

In Section 5.1, we chose a unitary frequency, or $f = 1$ (dimensionless), so that the wavenumber associated with the host medium Ω_2 becomes $k = \omega/c = 2\pi f\sqrt{\rho_2/K_2} = 2\pi$ (see Section 2.2). In testing the first inf-sup condition, the entries in matrix $\overline{\mathbb{A}}$ are calculated using this value for k. We plot the values $\sqrt{\sigma_{\min}(h,1)}$ from (36b) in Figure 12(A). They are all positive and stabilized around a positive value as h decreases, so that the third hypothesis (Section 7.3) is satisfied. In Figure 12(B) we plot the values $\sqrt{\tau_{\min}(h)}$ from (37b) relative to the second inf-sup condition. They are also all positive and stabilized at a positive value, so that the fourth hypothesis (Section 7.3) is satisfied. We conclude that the inf-sup test has been passed, or that this problem keeps its well-posedness as h decreases.

8.2 | Scattering by a kite-shaped object (Section 5.2)

For this example, we have $K_{test} = 9$. The sequence of finite sphere systems is such that the number of balls over Ω_1 varies from 64 to 275, the number of balls over Ω_2 varies from 389 to 1763, and the number of balls over $\Gamma_{1,2}$ varies from 31 to 67.

In Section 5.2, the incident plane wave has a frequency of $f = f_0 = 5$ kHz, so that the wavenumber of the problem is $k = k_0 = 20.81$ rad/m. When testing the first inf-sup condition, we consider a range of frequencies from 1.5 to 15 kHz, with increments of 500 Hz. For each value of frequency f, we determine the wavenumber $k = \omega/c = 2\pi f\sqrt{\rho_2/K_2}$ (see Section 2.2) and calculate the smallest eigenvalues $\sigma_{\min}(h, f)$ in (36b) for the sequence of $K_{test} = 9$ discretizations. The graph corresponding to the values $\sqrt{\sigma_{\min}(h,f)}$ is shown in Figure 13(A). We observe that for each frequency f, they are positive and stabilized around a positive value as h decreases. At any given point on the graph, there is variation in the direction of f, but not in the direction of h. The graph shows a profile with almost parallel lines along the h axis, as shown in Figure 13(A). The results allow us to conclude that

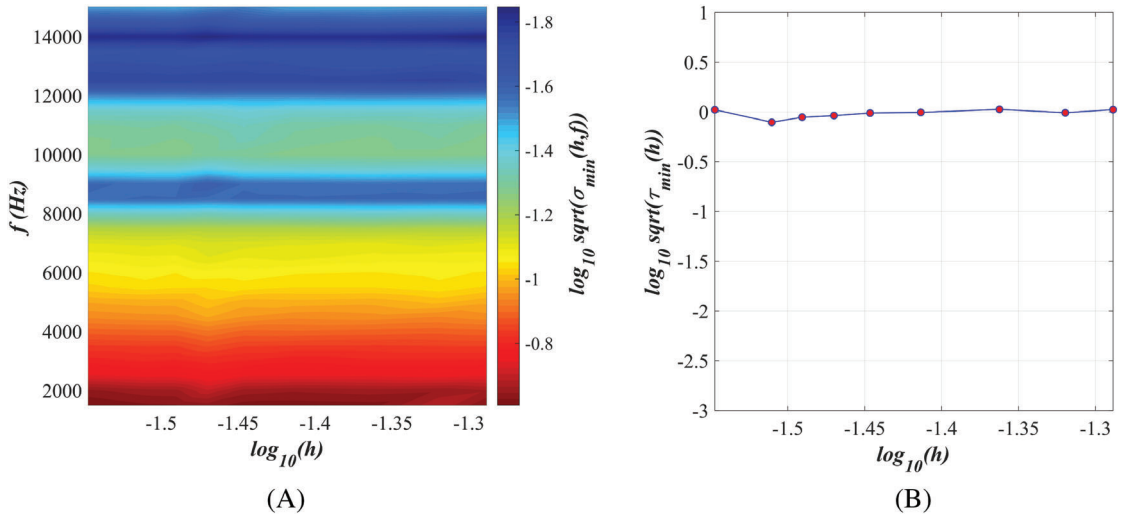

FIGURE 13 The inf-sup values, scattering by a kite-shaped object (Section 5.2). (A) First inf-sup condition, $\log_{10}\sqrt{\sigma_{\min}(h,f)}$ as a function of $\log_{10}h$ and f. (B) Second inf-sup condition, $\log_{10}\sqrt{\tau_{\min}(h)}$ as a function of $\log_{10}h$

for any given *fixed frequency* f, the inf-sup values do not decrease with h. In this way, for each fixed frequency f, the third hypothesis (Section 7.3) is satisfied. In Figure 13(B) we show the values $\sqrt{\tau_{\min}(h)}$ relative to the second inf-sup condition. They are all positive and stabilized at a positive value, so that the fourth hypothesis (Section 7.3) is satisfied. We therefore conclude that for the range of frequencies considered, the inf-sup test has been passed.

8.3 | Scattering by a cladded object (Section 5.3)

In this example, we use $K_{test} = 8$. The sequence of finite sphere systems is such that the number of balls over Ω_1 varies from 45 to 140, the number of balls over Ω_2 varies from 97 to 279, and the number of balls over Ω_3 varies from 274 to 821. In what concerns the interfaces, the number of balls over $\Gamma_{1,2}$ varies from 20 to 40, and the number of balls over $\Gamma_{2,3}$ varies from 37 to 67.

In Section 5.3, the incident plane wave has a frequency of $f = 3f_0 = 3$ kHz, so that the wavenumber of the problem is $k = 12.48$ rad/m. In order to test the first inf-sup condition, we consider a range of frequencies from 500 Hz to 5 kHz, with increments of 125 Hz. We proceed as in Section 8.2: For each value of frequency f, we find the wavenumber $k = \omega/c = 2\pi f\sqrt{\rho_3/K_3}$ (Section 2.2) and calculate the smallest eigenvalues $\sigma_{\min}(h, f)$ in (36b) for the sequence of $K_{test} = 8$ discretizations. The graph corresponding to the values $\sqrt{\sigma_{\min}(h,f)}$ is shown in Figure 14(A). For each frequency f, they are positive and stabilized around a positive value as h decreases. Therefore, for each *fixed frequency* f, the third hypothesis (Section 7.3) is satisfied. We observe the same pattern described in Section 8.2, that is, the values $\sqrt{\sigma_{\min}(h,f)}$ vary with f, but there is almost no variation with h (a parallel profile along the h axis). In Figure 14(B) we show the values $\sqrt{\tau_{\min}(h)}$ relative to the second inf-sup condition. They are all positive and stabilized at a positive value. It follows that the fourth hypothesis (Section 7.3) is satisfied. For this range of frequencies, the inf-sup test has been passed.

8.4 | Scattering by a group of objects (Section 5.4)

In this example, $K_{test} = 8$. The sequence of finite sphere systems is such that the number of balls over Ω_1 varies from 54 to 135, the number of balls over Ω_2 varies from 57 to 137, the number of balls over Ω_3 varies from 56 to 138, and the number of balls over Ω_4 varies from 767 to 2115. In what concerns the interfaces, the number of balls over $\Gamma_{1,4}$, $\Gamma_{2,4}$, and $\Gamma_{3,4}$ varies from 27 to 45.

In Section 5.4, the incident plane wave has a frequency of $f = f_0 = 4$ kHz, so that the wavenumber of the problem is $k = k_0 = 16.65$ rad/m. When testing the first inf-sup condition, we consider a range of frequencies from 2 kHz to 10 kHz,

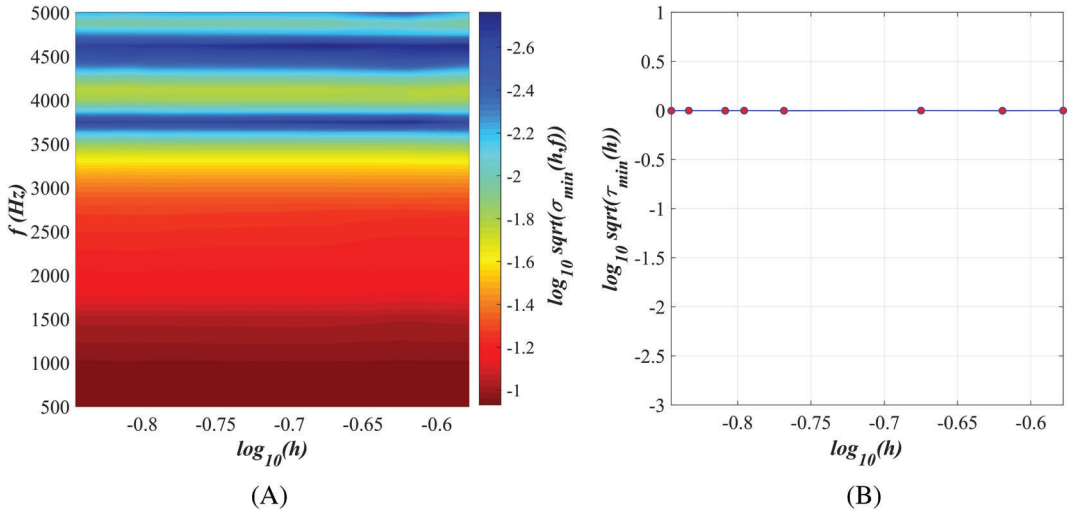

FIGURE 14 The inf-sup values, scattering by a cladded object (Section 5.3). (A) First inf-sup condition, $\log_{10}\sqrt{\sigma_{\min}(h,f)}$ as a function of $\log_{10}h$ and f. (B) Second inf-sup condition, $\log_{10}\sqrt{\tau_{\min}(h)}$ as a function of $\log_{10}h$

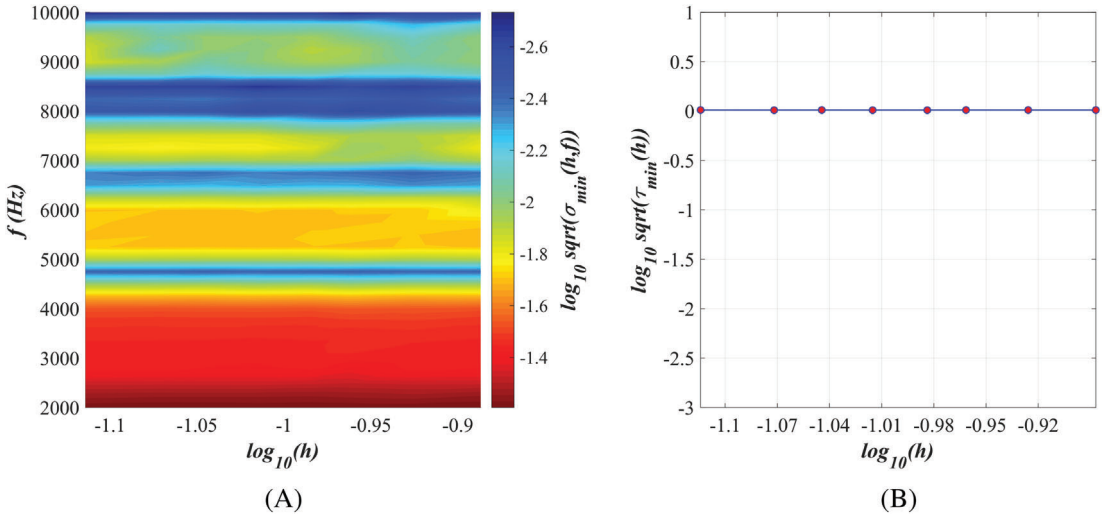

FIGURE 15 The inf-sup values, scattering by a group of objects (Section 5.4). (A) First inf-sup condition, $\log_{10}\sqrt{\sigma_{\min}(h,f)}$ as a function of $\log_{10}h$ and f. (B) Second inf-sup condition, $\log_{10}\sqrt{\tau_{\min}(h)}$ as a function of $\log_{10}h$

with increments of 250 Hz. The procedure is the same as that from Sections 8.2 and 8.3: For each value of frequency f, we find the wavenumber $k = \omega/c = 2\pi f\sqrt{\rho_4/K_4}$ (Section 2.2) and calculate the smallest eigenvalues $\sigma_{\min}(h, f)$ in (36b) for the sequence of $K_{test} = 8$ discretizations. In Figure 15(A) we plot the graph with the values $\sqrt{\sigma_{\min}(h,f)}$. For each frequency f, they are positive and stabilized around a positive value as h decreases. In this way, for each *fixed frequency* f, the third hypothesis (Section 7.3) is satisfied. We again observe the same pattern described in Sections 8.2 and 8.3, that is, the values $\sqrt{\sigma_{\min}(h,f)}$ vary with f, but there is almost no variation with h (the profile is essentially parallel to the h axis). Figure 15(B) shows the values $\sqrt{\tau_{\min}(h)}$ relative to the second inf-sup condition. They are all positive and stabilized at a positive value. Therefore the fourth hypothesis (Section 7.3) is satisfied. For the range of frequencies considered, the discretization passed the inf-sup test.

9 | CONCLUDING REMARKS

The focus of this work is on the design of a completely meshfree procedure able to deal with the problem of discontinuous gradients in acoustic scattering. The procedure does not depend on any kind of adjustable parameter. We used the MFS

as the underlying meshfree method, extending it for the first time to problems posed in nonhomogeneous media. Other meshfree methods could of course also be used as the underlying method. But the ease in constructing basis functions (no need for inverting matrices as in the moving-least squares shape functions[9]) and in incorporating local enrichment functions, together with its superior performance (as attested by a number of earlier works, see Section 1), make the MFS an attractive choice.

The discontinuous gradients are treated with Lagrange multipliers, and the final variational problem is written as a saddle-point problem (mixed formulation). The solutions provided by our method are in good agreement with those provided by the FEM, and the meshfree solutions present no oscillations close to the interface.

The second part of the paper deals with the inf-sup stability of the discrete mixed problems. The well-established general theory of inf-sup stability of mixed methods is specialized to our mixed formulation of the acoustic scattering problem, which is a two-field problem, posed in terms of the pressure fields and the Lagrange multiplier fields. Two inf-sup conditions are needed, since the standard bilinear form originating from the Helmholtz equation is not coercive. Based on stronger inf-sup conditions that are sufficient to imply the original conditions,[72] we move next to the linear algebraic level, and a subsequent application of the inf-sup test reveals that the discrete problems are inf-sup stable. A variety of geometries is investigated (considering both simply connected and not simply-connected domains).

In future works, different functions (e.g., plane waves) can be added to the collections of local enrichment functions[15] (in addition to the quadratic functions used here), as done for the OFE,[20,22] and their possible impact on the inf-sup stability of the discrete problems can be evaluated. The solution technique described in this paper can be extended to three-dimensional scattering problems,[16] but the required numerical operations may be large. Other directions of research include inquiries into the connection between the characteristics of the bilinear forms involved in our problem and the inf-sup constants.[96] Another line of investigation is the application of the proposed method to scattering problems posed in nonhomogeneous media in which the interfaces are open curves (as in Figure 2(B)). Despite the fact that the discretization procedures proposed in Section 4 could in principle yield good results, we point out that the treatment of open curves may lead to different function spaces. The Lagrange multiplier fields may no longer be elements of the Sobolev space $H^{-1/2}$, but may belong to the Lions-Magenes space $H_{00}^{-1/2}$ instead.[32] Since the derivation of the correct inf-sup conditions may depend on these spaces, further theoretical work is required.

ACKNOWLEDGMENTS

This research work was supported by the Brazilian Ministry of Education (CAPES/PNPD), and by the National Council for Scientific and Technological Development (CNPq), under grant 150699/2019-0.

DATA AVAILABILITY STATEMENT

Data sharing not applicable.

ORCID


Williams L. Nicomedes https://orcid.org/0000-0002-7928-8419

REFERENCES

1. Bathe KJ. *Finite Element Procedures*. Prentice Hall; 1996. 2nd ed. KJ Bathe, Watertown, MA; 2014 and Higher Education Press, China; 2016.
2. Ciarlet PG, Lions JL. *Handbook of Numerical Analysis*. Finite Element Methods (Part 1). Vol II. Amsterdam, The Netherlands: Elsevier Science B. V.; 1991.
3. Sevilla R, Rees L, Hassan O. The generation of triangular meshes for NURBS-enhanced FEM. *Int J Numer Methods Eng*. 2016;108:941-968.
4. Lin H, Jin S, Liao H, Jian Q. Quality guaranteed all-hex mesh generation by a constrained volume iterative fitting algorithm. *Comput Aided Des*. 2015;67-68:107-117.
5. Belytschko T, Black T. Elastic crack growth in finite elements with minimal remeshing. *Int J Numer Methods Eng*. 1999;45:601-620.
6. Shahani AR, Fasakhodi MRA. Finite element analysis of dynamic crack propagation using remeshing technique. *Mater Des*. 2009;30:1032-1041.
7. Formica G, Milicchio F. Crack growth propagation using standard FEM. *Eng Fract Mech*. 2016;165:1-18.
8. Sheng A, Ghoniem NM, Crosby T, Po G. A mesh-independent method for planar three-dimensional crack growth in finite domains. *Int J Numer Methods Eng*. 2019;117:38-62.
9. Liu GR. *Meshfree Methods: Moving Beyond the Finite Element Method*. 2nd ed. Boca Raton, FL: CRC Press; 2010.
10. Li S, Liu WK. *Meshfree Particle Methods*. New York, NY: Springer; 2007.
11. Monaghan JJ. An introduction to SPH. *Comput Phys Commun*. 1988;48:89-96.
12. Belytschko T, Lu YY, Gu L. Element-free Galerkin methods. *Int J Numer Methods Eng*. 1994;37:229-256.

13. Atluri S, Shen S. The meshless local Petrov-Galerkin method: a simple and less-costly alternative to the finite-element and boundary element methods. *CMES Comput Model Eng Sci*. 2002;3:11-51.
14. De S, Bathe KJ. The method finite spheres. *Comput Mech*. 2000;25:329-345.
15. Ham S, Lai B, Bathe KJ. The method of finite spheres for wave propagation problems. *Comput Struct*. 2014;142:1-14.
16. Nicomedes WL, Bathe KJ, Moreira FJS, Mesquita RC. Meshfree analysis of electromagnetic wave scattering from conducting targets: formulation and computations. *Comput Struct*. 2017;184:36-52.
17. Bathe KJ. The finite element method with 'overlapping finite elements'. Paper presented at the Proceedings of the 6th International Conference on Structural Engineering, Mechanics and Computation – SEMC 2016, (A. Zingoni, ed.); 2016. Cape Town, South Africa.
18. Bathe KJ, Zhang L. The finite element method with overlapping elements – a new paradigm for CAD driven simulations. *Comput Struct*. 2017;182:526-539.
19. Zhang L, Kim KT, Bathe KJ. The new paradigm of finite element solutions with overlapping elements in CAD – computational efficiency of the procedure. *Comput Struct*. 2018;199:1-17.
20. Kim KT, Zhang L, Bathe KJ. Transient implicit wave propagation dynamics with overlapping finite elements. *Comput Struct*. 2018;199:18-33.
21. Bathe KJ. The AMORE paradigm for finite element analysis. *Adv Eng Softw*. 2019;130:1-13.
22. Chai Y, Bathe KJ. Transient wave propagation in inhomogeneous media with enriched overlapping triangular elements. *Comput Struct*. 2020;237:1-20.
23. Gaul L, Kögl M, Wagner M. *Boundary Element Methods for Engineers and Scientists: An Introductory Course with Advanced Topics*. New York, NY: Springer; 2003.
24. Diwan GC, Trevelyan J, Coates G. A comparison of techniques for overcoming non-uniqueness of boundary integral equations for the collocation partition of unity method in two-dimensional acoustic scattering. *Int J Numer Methods Eng*. 2013;96:645-664.
25. Sutradhar A, Paulino GH. A simple boundary element method for problems of potential in non-homogeneous media. *Int J Numer Methods Eng*. 2004;60:2203-2230.
26. Ihlenburg F. *Finite Element Analysis of Acoustic Scattering*. Applied Mathematical Sciences Series. Vol 132. New York, NY: Springer; 1998.
27. Ham S, Bathe KJ. A finite element method enriched for wave propagation problems. *Comput Struct*. 2012;94:1-12.
28. Colton D, Kress R. *Inverse Acoustic and Electromagnetic Scattering Theory*. Applied Mathematical Sciences Series. Vol 93. 3rd ed. New York, NY: Springer; 2013.
29. Jensen FB, Kuperman WA, Porter MB, Schmidt H. *Computational Ocean Acoustics*. Modern Acoustics and Signal Processing Series. 2nd ed. New York, NY: Springer; 2011.
30. Aragón AM, Duarte CA, Geubelle PH. Generalized finite element enrichment functions for discontinuous gradient fields. *Int J Numer Methods Eng*. 2010;82:242-268.
31. Soghrati S, Aragón AM, Duarte CA, Geubelle PH. An interface-enriched generalized FEM for problems with discontinuous gradient fields. *Int J Numer Methods Eng*. 2012;89:991-1008.
32. Ferté G, Massin P, Moës N. Interface problems with quadratic X-FEM: design of a stable multiplier space and error analysis. *Int J Numer Methods Eng*. 2014;100:834-870.
33. Fries TP, Belytschko T. The extended/generalized finite element method: an overview of the method and its applications. *Int J Numer Methods Eng*. 2010;84:253-304.
34. Bathe KJ, Khoshgoftaar MR. Finite element free surface seepage analysis without mesh iteration. *Int J Numer Anal Methods Geomech*. 1979;3:13-22.
35. Zou Z, Aquino W, Harari I. Nitsche's method for Helmholtz problems with embedded interfaces. *Int J Numer Methods Eng*. 2017;110:618-636.
36. Diwan GC, Mohamed MS, Seaid M, Trevelyan J, Laghrouche O. Mixed enrichment for the finite element method in heterogeneous media. *Int J Numer Methods Eng*. 2014;101:54-78.
37. Moës N, Béchet E, Tourbier M. Imposing Dirichlet boundary conditions in the extended finite element method. *Int J Numer Methods Eng*. 2006;67:1641-1669.
38. El-Abbasi N, Bathe KJ. Stability and patch test performance of contact discretizations and a new solution algorithm. *Comput Struct*. 2001;79:1473-1486.
39. Brezzi F, Bathe KJ. A discourse on the stability conditions for mixed finite element formulations. *Comput Methods Appl Mech Eng*. 1990;82:27-57.
40. Brezzi F, Fortin M. *Mixed and Hybrid Finite Elements*. Springer Series in Computational Mathematics. Vol 15. New York, NY: Springer; 1991.
41. Boffi D, Brezzi F, Fortin M. *Mixed Finite Element Methods and Applications*. Springer Series in Computational Mathematics. Vol 44. New York, NY: Springer; 2013.
42. Hautefeuille M, Annavarapu C, Dolbow JE. Robust imposition of dirichlet boundary conditions on embedded surfaces. *Int J Numer Methods Eng*. 2012;90:40-64.
43. Ji H, Dolbow JE. On strategies for enforcing interfacial constraints and evaluating jump conditions with the extended finite element method. *Int J Numer Methods Eng*. 2004;61:2508-2535.
44. Hansbo P, Lovadina C, Perugia I, Sangalli G. A Lagrange multiplier method for the finite element solution of elliptic interface problems using non-matching meshes. *Numer Math*. 2005;100:91-115.

45. Béchet E, Moës N, Wohlmuth B. A stable Lagrange multiplier space for stiff interface conditions within the extended finite element method. *Int J Numer Methods Eng*. 2009;78:931-954.
46. Chazot JD, Nennig B, Perrey-Debain E. Performances of the partition of unity finite element method for the analysis of two-dimensional interior sound fields with absorbing materials. *J Sound Vib*. 2013;332:1918-1929.
47. Farhat C, Kalashnikova I, Tezaur R. A higher-order discontinuous enrichment method for the solution of high Péclet advection-diffusion problems on unstructured meshes. *Int J Numer Methods Eng*. 2010;81:604-636.
48. Kalashnikova I, Tezaur R, Farhat C. A discontinuous enrichment method for variable-coefficient advection-diffusion at high Péclet number. *Int J Numer Methods Eng*. 2011;87:309-335.
49. Huynh LNT, Nguyen NC, Peraire J, Khoo BC. A high-order hybridizable discontinuous Galerkin method for elliptic interface problems. *Int J Numer Methods Eng*. 2013;93:183-200.
50. Brandstetter G, Govindjee S. A high-order immersed boundary discontinuous-Galerkin method for Poisson's equation with discontinuous coefficients and singular sources. *Int J Numer Methods Eng*. 2015;101:847-869.
51. Li BQ. *Discontinuous Finite Elements in Fluid Dynamics and Heat Transfer*. Computational Fluid and Solid Mechanics Series. London: Spinger-Verlag; 2006.
52. Ben Belgacem F. The mortar finite element method with Lagrange multipliers. *Numer Math*. 1999;84:173-197.
53. Wohlmuth BI. A mortar finite element method using dual spaces for the Lagrange multiplier. *SIAM J Numer Anal*. 2000;38:989-1012.
54. Babuska I, Banerjee U, Osborn JE. Survey of meshless and generalized finite elements: a unified approach. *Acta Numer*. 2003;12:1-125.
55. Nicomedes WL, Mesquita RC, Moreira FJS. The meshless local Petrov-Galerkin method in two-dimensional electromagnetic wave analysis. *IEEE Trans Antennas Propag*. 2012;60:1957-1968.
56. Nicomedes WL, Mesquita RC, Moreira FJS. Calculating the band structure of photonic crystals through the meshless local Petrov-Galerkin (MLPG) method and periodic shape functions. *IEEE Trans Magnet*. 2012;48:551-554.
57. Yu Y, Chen Z. Towards the development of an unconditionally stable time-domain meshless method. *IEEE Trans Microw Theory Techn*. 2010;58:578-586.
58. Krongauz Y, Belytschko T. EFG approximation with discontinuous derivatives. *Int J Numer Methods Eng*. 1998;41:1215-1233.
59. Zhang Z, Noguchi H, Chen JS. Moving least-squares approximation with discontinuous derivative basis functions for shell structures with slope discontinuities. *Int J Numer Methods Eng*. 2008;76:1202-1230.
60. Batra RC, Porfiri M, Spinello D. Treatment of material discontinuity in two meshless local Petrov-Galerkin (MLPG) formulations of axisymmetric transient heat conduction. *Int J Numer Methods Eng*. 2004;61:2461-2479.
61. Zheng H, Li W, Du X. Exact imposition of essential boundary condition and material interface continuity in Galerkin-based meshless methods. *Int J Numer Methods Eng*. 2017;110:637-660.
62. De S, Bathe KJ. Displacement/pressure mixed interpolation in the method of finite spheres. *Int J Numer Methods Eng*. 2001;51:275-292.
63. De S, Bathe KJ. The method of finite spheres with improved numerical integration. *Comput Struct*. 2001;79:2183-2196.
64. De S, Bathe KJ. Towards an efficient meshless computational technique: the method of finite spheres. *Eng Comput*. 2001;18:170-192.
65. De S, Hong JW, Bathe KJ. On the method of finite spheres in applications: towards the use with ADINA and in a surgical simulator. *Comput Mech*. 2003;31:27-37.
66. Macri M, De S. Towards an automatic discretization scheme for the method of finite spheres and its coupling with the finite element method. *Comput Struct*. 2005;83:1429-1447.
67. De S, Kim J, Lim YJ, Srinivasan MA. The point collocation-based method of finite spheres (PCMFS) for real time surgery simulation. *Comput Struct*. 2005;83:1515-1525.
68. Hong JW, Bathe KJ. Coupling and enrichment schemes for finite element and finite sphere discretizations. *Comput Struct*. 2005;83:1386-1395.
69. BaniHani SM, De S. On the evaluation of the method of finite spheres for the solution of Reissner-Mindlin plate problems using the numerical inf-sup test. *Int J Numer Methods Eng*. 2007;70:1366-1386.
70. Kim KT, Bathe KJ. Transient implicit wave propagation dynamics with the method of finite spheres. *Comput Struct*. 2016;173:50-60.
71. Lai B, Bathe KJ. The method of finite spheres in three-dimensional linear static analysis. *Comput Struct*. 2016;173:161-173.
72. Nicomedes WL, Bathe KJ, Moreira FJS, Mesquita RC. The method of finite spheres in acoustic wave propagation through nonhomogeneous media: Inf-sup stability conditions. *Vietnam J Mech*. 2020;42:209-237.
73. McLean W. *Strongly Elliptic Systems and Boundary Integral Equations*. Cambridge, MA: Cambridge University Press; 2000.
74. Grisvard P. *Elliptic Problems in Nonsmooth Domains*. SIAM Classics in Applied Mathematics. Vol 69. Philadelphia, PA: Society for Industrial and Applied Mathematics (SIAM); 2011.
75. Boyer F, Fabrie P. *Mathematical Tools for the Study of the Incompressible Navier-Stokes Equations and Related Models*. Applied Mathematical Sciences Series. Vol 183. New York: Springer-Verlag; 2013.
76. Peterson AF, Ray SL, Mittra R. *Computational Methods for Electromagnetics*. Hoboken, NJ: Wiley-IEEE Press; 1998.
77. Evans LC. *Partial Differential Equations*. Graduate Studies in Mathematics. Vol 19. 2nd ed. Providence, RI: American Mathematical Society; 2010.
78. Leoni G. *First Course in Sobolev Spaces*. Graduate Studies in Mathematics. Vol 181. 2nd ed. Providence, RI: American Mathematical Society; 2017.
79. Adams RA, Fournier JJF. *Sobolev Spaces*. Pure and Applied Mathematics. Vol 140. 2nd ed. Amsterdam, The Netherlands: Academic Press, Elsevier B. V.; 2003.

80. Ciarlet PG. *Linear and Nonlinear Functional Analysis with Applications*. Philadelphia, PA: Society for Industrial and Applied Mathematics (SIAM); 2013.
81. Nédélec JC. *Acoustic and Electromagnetic Equations: Integral Representations for Harmonic Problems*. Applied Mathematical Sciences Series. Vol 144. New York, NY: Springer; 2001.
82. Chapelle D, Bathe KJ. *The Finite Element Analysis of Shells – Fundamentals*. 2nd ed. New York, NY: Springer; 2011.
83. Dziuk G, Elliott CM. Finite element methods for surface PDEs. *Acta Numerica*. 2013;22:289-396.
84. Schweitzer B. *Partielle Differential-gleichungen Eine anwendungsorientierte Einführung. 2 Auflage*. New York, NY: Springer; 2018.
85. Ern A, Guermond JL. *Theory and Practice of Finite Elements*. Applied Mathematical Sciences Series. Vol 159. New York, NY: Springer; 2004.
86. Gatica GN. *A Simple Introduction to the Mixed Finite Element Method: Theory and Applications*. Springer Briefs in Mathematics. New York, NY: Springer; 2014.
87. Chapelle D, Bathe KJ. On the ellipticity condition for model-parameter dependent mixed formulations. *Comput Struct*. 2010;88:581-587.
88. Moiola A, Spence EA. Is the Helmholtz equation really sign-indefinite? *SIAM Rev*. 2014;56:274-312.
89. Chapelle D, Bathe KJ. The inf-sup test. *Comput Struct*. 1993;47:537-545.
90. Bathe KJ. The inf-sup condition and its evaluation for mixed finite element methods. *Comput Struct*. 2001;79:243-252.
91. Bao W, Wang X, Bathe KJ. On the inf-sup condition of mixed finite element formulations for acoustic fluids. *Math Models Methods Appl Sci*. 2001;11:883-901.
92. Iosilevich A, Bathe KJ, Brezzi F. On evaluating the inf-sup condition for plate bending elements. *Int J Numer Methods Eng*. 1997;40:3639-3663.
93. Bathe KJ, Hendriana D, Brezzi F, Sangalli G. Inf-sup testing of upwind methods. *Int J Numer Methods Eng*. 2000;48:745-760.
94. Bathe KJ, Iosilevich A, Chapelle D. An inf-sup test for shell finite elements. *Comput Struct*. 2000;75:439-456.
95. Ko Y, Bathe KJ. Inf-sup testing of some three-dimensional low-order finite elements for the analysis of solids. *Comput Struct*. 2018;209:1-13.
96. Demkowicz L. Asymptotic convergence in finite and boundary element methods: Part 1: theoretical results. *Comput Math Appl*. 1994;27:69-84.
97. Salsa S. *Partial Differential Equations in Action: From Modelling to Theory*. 3rd ed. New York, NY: Springer; 2016.

How to cite this article: Nicomedes WL, Bathe KJ, Moreira FJS, Mesquita RC. Acoustic scattering in nonhomogeneous media and the problem of discontinuous gradients: Analysis and inf-sup stability in the method of finite spheres. *Int J Numer Methods Eng*. 2021;122:3141–3170. https://doi.org/10.1002/nme.6647

APPENDIX A. THE TRACE THEOREM

Let D be an open and bounded subset of $\mathbb{R}^2$. We introduce the spaces of continuous functions[77]:

$$C(D) \overset{\text{def}}{=} \{u : D \longrightarrow \mathbb{C} \mid u \text{ is continuous on } D\}, \tag{A1}$$

$$C^1(D) \overset{\text{def}}{=} \{u \in C(D) \mid \partial u/\partial x, \partial u/\partial y \in C(D)\}, \tag{A2}$$

$$C(\overline{D}) \overset{\text{def}}{=} \left\{ u \in C(D) \mid \sup_{\boldsymbol{x}\in D} u(\boldsymbol{x}) < \infty \right\}, \tag{A3}$$

$$C^{0,1}(\overline{D}) \overset{\text{def}}{=} \left\{ u \in C(\overline{D}) \mid \sup_{\substack{\boldsymbol{x},\boldsymbol{y}\in D \\ \boldsymbol{x}\neq\boldsymbol{y}}} \frac{|u(\boldsymbol{x}) - u(\boldsymbol{y})|}{|\boldsymbol{x} - \boldsymbol{y}|} < \infty \right\}. \tag{A4}$$

In (A3), $\overline{D} = D \cup \partial D$. If $u \in C(\overline{D})$, then u can be continuously extended to the boundary,[97] that is, there exists a function $\widetilde{u} : \overline{D} \longrightarrow \mathbb{R}$ such that $\widetilde{u}|_D = u$. Moreover, for any point $\boldsymbol{x} \in \partial D$ and any sequence of points $(\boldsymbol{y}_n)_{n\in\mathbb{N}}$ in D converging to $\boldsymbol{x}$, the limit $\lim_{n\to\infty} u(\boldsymbol{y}_n)$ is well-defined, and we can define $\widetilde{u}(\boldsymbol{x}) \overset{\text{def}}{=} \lim_{n\to\infty} u(\boldsymbol{y}_n)$. The Trace theorem[74,75,97] affirms that if D is a bounded and open subset of $\mathbb{R}^2$ with a Lipschitz continuous boundary ∂D, then there is a continuous linear operator $\gamma_{\partial D} : H^1(D) \longrightarrow L^2(\partial D)$, whose image is $H^{1/2}(\partial D) \subset L^2(\partial D)$, and such that $\gamma_{\partial D}(u) = \widetilde{u}|_{\partial D}$, for any $u \in H^1(D) \cap C^{0,1}(\overline{D})$.

APPENDIX B. THE SPACE $H^{1/2}$

Let D be an open and bounded subset of $\mathbb{R}^2$ with Lipschitz continuous boundary ∂D. A function $t \in L^2(\partial D)$ belongs to the fractional Sobolev space $W^{1/2,2}(\partial D)$, usually denoted by $H^{1/2}(\partial D)$, if the Slobodeckij seminorm

$$|t|_{H^{1/2}(\partial D)} \stackrel{\text{def}}{=} \left(\int_{\partial D} \int_{\partial D} \frac{|t(\boldsymbol{x}) - t(\boldsymbol{y})|^2}{\|\boldsymbol{x} - \boldsymbol{y}\|^2} d\Gamma_{\boldsymbol{x}} d\Gamma_{\boldsymbol{y}} \right)^{\frac{1}{2}} \tag{B1}$$

is finite, where $d\Gamma_{\boldsymbol{x}}$ and $d\Gamma_{\boldsymbol{y}}$ denote the length measure on ∂D parametrized by $\boldsymbol{x}$ and $\boldsymbol{y}$, respectively.[78] The norm in $H^{1/2}(\partial D)$ is given by.

$$\|t\|_{H^{1/2}(\partial D)} \stackrel{\text{def}}{=} (\|t\|^2_{L^2(\partial D)} + |t|^2_{H^{1/2}(\partial D)})^{\frac{1}{2}}. \tag{B2}$$

For any $t \in H^{1/2}(\partial D)$ and for any subset $\Gamma_0 \subset \partial D$ (with nonzero measure), it follows from (B1) that the restriction of t to Γ_0 belongs to $H^{1/2}(\Gamma_0)$, that is, $t|_{\Gamma_0} \in H^{1/2}(\Gamma_0)$.